An ensemble of meteorological stations for estimating daily air temperature time series at Jungfraujoch since 1864

Marco Bongio[1,2], Riccardo Scotti[2], Carlo De Michele[1]

[1]Department of Civil and Environmental Engineering, Politecnico di Milano, Piazza Leonardo da Vinci 32, 20133, Milano, Italy

[2]Servizio Glaciologico Lombardo, Via Statale 43, 23888 La Valletta Brianza (LC), Italy, riccardoscotti80@gmail.com

Correspondence to: Bongio Marco (marco.bongio@polimi.it) and Carlo De Michele (carlo.demichele@polimi.it)

Keywords: temperature, high elevation sites, statistical model, long-term daily temperature series, long term temperature, temperature lapse rate.

Abstract. Air temperature is a pivotal variable influencing numerous chemical, physical, and biological processes. However, there is a notable scarcity of long-term data, especially at high elevations, exceeding 2000 m a.s.l. This study focuses on reconstructing the daily maximum, mean, and minimum temperatures at Jungfraujoch (3571 m a.s.l.) since 1864. The approach involves daily data from ten meteorological stations within the ECA&D (6) and Meteo Swiss (4) databases. All selected stations are located at an elevation above 2000 m a.s.l. (in the range 2140-3109 m a.s.l.), providing uninterrupted observations spanning at least from 1961 to 2022. The proposed methodology includes the following steps: 1) for each meteorological station, in the calibration period 1980-1999, it was modeled the daily temperature at Jungfraujoch as the sum of the temperature at the selected station plus a deterministic and a stochastic component. The seasonality requires parameters with monthly variability which are different considering maximum, mean, and minimum temperature; 2) Then the 10 simulated time series at Jungfraujoch defined an "ensemble" daily temperature time series, as the mean of them; 3) Model's performances was evaluated within two validation periods, 1961-1979 and 2000-2022 with correlation coefficients higher than 0.9 in both of them; 4) A further validation was made with the comparison between the "ensemble" mean daily temperature from 1864 and that estimated by Imfeld et al. 2023.

Comparing the results with the existing literature, we highlighted: i) high performances without the need of modeling the observed trend due to the climate change (subjected to high uncertainty in the future), ii) very parsimonious model without the need of any other variables (relative humidity, cloud cover, wind velocity, weather patterns); iii) the importance of selecting stations at high elevation (above 2000 m a.s.l.) rather than considering closer (but lower elevation) stations, which may be subjected to the thermal inversion phenomenon or local factors; iv) the maximum temperature is affected by higher errors, especially from 2000-2022, which is probably due to the higher increasing of the summer and winter temperatures at high elevation accordingly to an elevation warming dependence; v) The method could be easily extended to other regions and these results could be used to make a backward analysis of many environmental processes (glacio-hydrological and permafrost), within the Jungfrau-Aletsch UNESCO World Heritage Site.

1. INTRODUCTION

Air temperature is a measure of the thermal energy of the atmosphere and is mainly determined by the amount of solar radiation, which is absorbed by the Earth's surface, and re-emitted with an increased longwave trapped in the troposphere by the greenhouse gases. Atmospheric and oceanic circulation and currents redistribute the heat across the Earth surface defining the shape of the regional temperature patterns. Air temperature affects many Earth system processes and phenomena:1) life cycles and traits' evolution including physical, physiological and behavioral characteristics that favor organisms to regulate their body temperatures and survive within their geographic ranges (Sheldon and Tewksbury, 2014); 2) the rate of biological reactions, and enzymes' function needed for photosynthesis, respiration and other processes essential for survival (Smith and Dukes 2013); 3) it is the main driver of the hydrological cycle, determining the clouds formation, the precipitation occurrence and the extent of snow and ice cover (Barnett et al. 2005, Kleidon and Renner 2013, Beniston et al. 2018). 4) The rate and direction of chemical reactions, including those in rocks, soil, water and atmosphere (Shepherd 2003, Ahmad and Rasul 2008, Romeo et al 2015); 5) The amount of oxygen levels in the water and the frequency and intensity of fires (https://ugc.berkeley.edu/background-content/temperature/). From manual measurements with a simple thermometer in the past to modern remote sensing measurements with satellites, which enable real-time spatial coverage, monitoring air temperature is crucial, especially for studying the impacts of climate change on mountain environments.

Collected and stored over long timescales, observational data form the foundation of science and these historical records reflect the memory of past weather conditions. High-quality time series data of meteorological observations, spanning over decades, or even centuries, allow scientists to study and understand the Earth's climate, including its variations and trends (WMO 2022).

Climate change and rising temperature are not uniformly distributed worldwide and certain regions are "climatic hotspots". This is particularly true for the Mediterranean Region (Cos et al. 2022), the Arctic Region (Rantanen et al. 2022) and the European Alps (Gobiet et al. 2014). In recent decades, the warming in the Arctic has been much faster than in the rest of the world, a phenomenon known as Arctic amplification. The warming for high-elevation sites is linearly proportional to the temperature lapse rates (TLRs) along altitudinal and latitudinal gradients (Wang et al. 2016). This is a consequence of the functional shape of the Stefan-Boltzmann law in both vertical and latitudinal directions (Wang et al. 2016).

During the past decades, the Alpine climate has been subjected to distinctive long-term trends consistent with the global climate response to increasing GHG concentrations. From the late 19th century until the end of the 20th century, Alpine temperatures have risen at a rate about twice as large as the Northern Hemisphere average, resulting in a total annual mean temperature increase of about 2°C (Auer et al 2007). The observed warming was particularly pronounced from 1980 onwards, with annual mean warming rates of about 0.5°C per decade. This acceleration, that is recorded even at planetary scale, is primarily attributed to water vapor-enhanced greenhouse warming (Beniston et al 2005, Philipona, 2013, Gobiet et al. 2014).

Given the considerable temporal storage of water in form of snow and ice in the higher regions of the Alps, changes in high elevation climate are of particular interest for research on climate-related hydrological impacts in Alpine catchments (IPCC 2019). Observational evidence suggests that near surface temperature

trends can considerably depend on elevation, with higher rates of warming often found at high elevations (Gobiet et al 2014). This rule of thumb, however, is not always true and depends on the region and period under consideration (Rangwala and Miller 2012). The reasons for elevation-dependent temperature trends are manifold and include changes in large scale atmospheric circulation (Ceppi et al. 2012), as well as elevation-dependent changes in the surface energy balance induced by snow cover changes (Kotlarski et al. 2012; Scherrer et al., 2012), or changes in downward radiation fluxes following changes in atmospheric transmissivity (Philipona 2013).

Anomalously strong warming at low elevations in autumn and early winter, along with above-average spring temperature trends at elevations close to the snow line is attributed to the declining of the snow cover and an amplification due to the snow albedo feedback (Sherrer et al. 2012, Ceppi et al. 2012).

The temperature and precipitation data from in situ stations in mountain regions, along with global gridded data sets (observations, reanalysis, and model hindcasts) are used to investigate the elevation dependency of temperature and precipitation changes since 1900 (Pepin et al. 2022). Whilst the concept of elevation-dependent warming (EDW), whereby warming rates are stratified by elevation, is widely accepted, no consistent EDW profile at the global scale has been identified, but when a local comparison was made, mountain sites are usually warming faster than lower areas nearby (Mountain Research Initiative EDW Working Group, 2015).

The combination of enhanced mountain warming, and reduced elevation dependency of rainfall/snowfall could cause a faster than previously assumed decline of mountain snow and ice (Pepin et al. 2022). In addition, Tudoroiu et al., (2016), found an even negative elevation dependent warming trend over the Eastern Alps, consistent for mean, maximum and minimum air temperature. The reason of this was found on the increasing global radiation at low elevations, and land cover and land use changes (abandonment of alpine pastures, expansion of secondary forest succession), which are local factors avoiding easy generalizations (Ohmura, 2012).

Within the Switzerland territory, due to the high quality of the meteorological station network, in terms of high spatial resolution and standardized and homogenized daily temperature time series, many studies had aimed to define gridded dataset of the whole territory. Meteo Swiss provided it for the period 1961-2020 (Meteo Swiss Spatial Climate Analyses, 2021). Pfister et al. (2020) provided a continuous spatial weather reconstruction for daily precipitation and temperature since 1864. They used an analogue resampling method (ARM) using station data and a weather type classification. An ensemble Kalman fitting approach and a quantile mapping were then applied in post processing. This is the first example of a dynamical and stochastic model which can offer new possibilities to make use of sparse information and enable to create spatial reconstruction of the past weather. Pfister et al. (2020) provided an open-source dataset (with 2.2 m resolution) repository on PANGAEA (https://doi.pangaea.de/10.1594/PANGAEA.907579). This dataset was then extended by Imfeld et al. (2023), defining a dataset of 258 years of daily temperature and precipitation fields for Switzerland from 1763 to 2020. This dataset was reconstructed with the analogue resampling method, based on the most similar day in a reference period. These fields are subsequently refined with data assimilation for temperature and bias correction for precipitation. Satisfactory validation results were founded prior to 1800 especially in the Swiss plateau (Imfeld et al. 2023).

Methods based on temperature lapse rates to reconstruct temperatures at high elevations are commonly used in the literature, and here they were analyzed for comparison. Commonly the WMO defines the dry adiabatic TLR at -1°C/100 m and a slower absolute value when cloudy or rainy days with high humidity rate persists (wet adiabatic value equal to -0.4°C/100m), but local conditions can have a strong influence on the temperature variability, such as in case of the thermal inversion typical for the winter season, with high diurnal temperature for steep slopes, brightened by the sun and cool pool air persisting on the valley bottom. The land cover can modify the temperature pattern, especially when the presence of snow abruptly increased the surface albedo, compared to rocks or bare soils, which absorb and re-emitted in a modified range of wavelength the solar radiation. The environmental lapse rate (ELR) of -0.65°C/100 m is commonly adopted as global mean value, and used in any modelling involving the use of climatic variables, such as hydrological models and mass balance snow and glacier simulations.

Rolland (2003) focusing on several regions on Northern Italy, found a seasonal pattern in monthly gradient variations with steepest lapse rate during summer about the maximum temperature. In the South-Central Idaho region (USA), Blandford (2008) recommended the use of the monthly lapse rate as a practical combination of the effective performance and ease of implementation. Winter air masses tend to be associated with steeper lapse rates from maximum temperature and drier air masses rather than minimum temperature and wet conditions, which experience shallower lapse rates.

A comparison of TLRs between northern and southern slopes of the Himalayas was made by Kattel et al. (2015). They found a distinct seasonal pattern of the TLR (steepest in winter and shallowest in summer), because in response to the monsoonal effect, the release of latent heat of water vapor condensation causes an increase in air temperature at high elevations.

The steepest TLR occurs in winter, in association with intense cooling at higher elevations, corresponding to the continental dry and cold surges, and considerable snow-temperature feedback. The observed contrast of winter TLR from northern to southern slopes of the Himalayas is due to the differences in elevations and topography as well as the pronounced effect of cold air surges. In the last decade, more complex models were developed to best define the spatial temperature gradients. To model non linearities in the vertical thermal profile, Frei (2014) defined non-linear parametric function and a distance-weighting scheme with a non-Euclidean metric that accounts for terrain effects for the spatial variability. Improvements are found on the temperature patterns from basin-scale inversion with valley-scale cold air pools and foehn situations. Jobst et al. (2017) defined a novel method to tackle the low station density at high elevations and high temperature variability using a trivariate thin-plate spline model constrained to the elevations of the continuous network, and two TLR methods to scale air temperature above the first layer. These latter two were based on the dominant processes during lapse-rate variation: cold air ponding and spatial differences in relative humidity.

Navarro-Serrano et al. (2018) analyzed the spatial and temporal variability of near surface lapse rate (NSLR) for continental Spain and their relationship to synoptic atmospheric circulation focusing on major mountain areas. The results showed that the NSLR varied markedly at spatial and seasonal scales and is depended on the dominant atmospheric conditions. They before calculated the median value for each subregion, which spanned from -5.80°C/Km to -4.67°C/Km less than the commonly used one of -

6.5°C/Km. Inland heating and thermal inversions are responsible of the lowest values. Because of the high errors on the estimation of daily temperature, simply using a fixed value of the Environmental lapse rate, they suggest a method to account at the daily weather type classification and the monthly variability.

Lute and Abatzoglou (2021) defined a guidance on best practices for estimating the lapse rate. They suggested to use a simple linear model rather than multiple linear regressions, and stations which can be considered topo-climatically similar. Temperature's estimations errors arise when small sample size (<5 years) or datasets with high noise or collinearity were considered.

The present work is focused on the reconstruction of the daily maximum, mean and mean temperature time series from 1864 at the Jungfraujoch (Switzerland). This latter was chosen because is the highest meteorological station within the Swiss territory and is the reference of the ICOS network about the greenhouse gases monitoring (Cristofanelli et al 2023). Within the Aletsch Unesco world Heritage site, where the cryospheric components are pivotal factors for many environmental and biological processes, the peculiarity of its location makes the reconstruction of the daily temperature a reference for a backward analysis of the high elevation sites.

Since mountains provide vital water resources to a significant proportion of the global population (Viviroli et al. 2007, 2011, Beniston and Stoffel 2014, Caty et al. 2018, Immerzeel et al. 2020), monitoring and protecting these resources from the combined impacts of growing demands and climate change is fundamental (Gleeson & Greenwood 2015; Singh & Thadani 2015, IPCC 2019). Motivations at the base of this study are: i) Make long-term temperature monitoring of mountain sites, as the Jungfraujoch; ii) Close the gap related to the lack of meteorological observations, affecting areas at high elevations. iii) Reconstruct the daily temporal time series of minimum, maximum and mean daily temperature at high elevations using stations at lower elevations and estimating the TLR parameter with monthly variability with a deep analysis of the residuals allows to define a low data requirements procedure without the need of any other observed variable, making this method easily expandable over other mountain chains. The use of an ensemble of stations is mandatory to obtain affordable results, especially when meteorological stations may present some missing data or problems.

In the next, data descriptions and preliminary analysis are given in section 2, methods in section 3, results and discussion in section 4, conclusions and open issues in section 5.

2. DATA DESCRIPTION AND PRELIMINARY ANALYSIS

This work is focused on the European Alps, a 200 km wide and 800 km long mountain range extending from about 44 to 48 °N and 3 to 16.5°E. The highest peaks reach 4800 m a.s.l. (Monte Bianco), and its average elevation is approximately 2500 m. North Atlantic weather systems, the Mediterranean Sea and the large Eurasian land mass influence climate variability in the European Alps (Bohm et al., 2001; Beniston and Jungo, 2002; Begert et al., 2005; Auer et al., 2005). The North Atlantic Oscillation (NAO; Wanner et al., 2001; Hurrell et al., 2003) is the dominant climate mode for Europe, particularly controlling the weather patterns in western and northern Europe (Auer et al., 2001).

The focus is the reconstruction of the maximum, mean, and minimum daily temperature at Jungfraujoch from 1864 (called in the following sections as target station TS) with an ensemble of 10 meteorological

stations (called in the following sections as backup stations BS). Daily temperature data come from two databases: 6 time series from ECA&d (European Climate Assessment & Dataset) and 4 retrieved from the Meteo Swiss. The position and the observation period for each of them are reported in Table 1 and Figure 1. The choice of the Jungfraujoch as a target site, and of each meteorological station was made after a deep investigation of the major daily databases such as GHCNd, ECA&d, Meteo Swiss. The target site of the Jungfraujoch was chosen because is the highest meteorological station within the Swiss territory and is the reference of the ICOS network about the greenhouse gases monitoring (Cristofanelli et al 2023). The peculiarity of its location, within the Aletsch Unesco world Heritage site, where the cryospheric components are a pivotal factor for many environmental and biological processes, makes the reconstruction of the daily temperature a reference for a backward analysis of the high elevation sites. The 10 sites were selected accordingly to the completeness of each time series at least from the year 1961. Common features of the 10 sites are: everyone is situated within the European Alps; they are positioned at an elevation above 2000 m; they are far from water body (lakes), they are positioned above a mountain ridge or a crest; they aren't influenced by glacier katabatic winds, which characterize ice-covered surfaces; they are far from obstacles or slopes which can exercise a shadow effect. The selection of meteorological stations is a fundamental factor especially in mountain regions, because it's mandatory to avoid some problems, which heavily affected the observed time series of temperature: the lack of the solar reflection screening which increases the maximum spring temperature when the snowpack persists above the ground and the solar radiation starts to grow; the persistence of cold air or wet air masses near a valley bottom, the thermal inversion phenomena typical for the winter season or during fohn events. From the existing literature, and about the Swiss territory, Frei (2014) found a non-linear vertical variation of the temperature with topographic height. In particular, within a very specific altitudinal range (generally from 1000 to 2000 m), he observed a sinusoidal increasing of the temperature with the elevation. This is the primary reason which suggests to avoid the use of the closest stations at the Jungfraujoch but placed in a range of elevation which can be affected by valley-scale and cold-air pools effects which can abruptly decrease the correlation between two meteorological stations positioned at different elevations. Before a detail description of the method section, a deep analysis of the observed time series was made. The data analysis consists on: i) quality check and calculation of the number of inconsistent or not available daily measurements with exclusion of time series with more than 5% of No data; ii) Focusing on the observation period 1961-2022, for each site, the yearly mean annual value time series of maximum, mean, minimum, temperature was calculated, and a moving average of 5 years was defined; iii) Based on the yearly moving average time series, a linear regression model was fitted within the period 1961-2022 and also, accordingly to the WMO's guidelines, the same method was applied within the two thirty years period 1961-1990 and 1991-2022; iv) The trend's significance was tested accordingly to the rejection of the null hypothesis of constant model with a p-value less than 0.1. Stationarity of the mean annual temperature time series was finally tested with the change point detection procedure (findchangepts Matlab function). v) Finally, among the different sites we compared the different trends and we investigate the presence of Elevation Dependent Warming (EDW). Parameters of the linear regression model, performances and the year of the changing point detected were described in Table S1 (Supplementary Materials). This analysis of the 1961-2022 period shows the non-

stationarity of the mean annual temperature time series, with higher increasing of the maximum temperature rather than mean and minimum ones for all of the meteorological stations (Figure S1 and S2 Supplementary Materials). The fitted trend rates span from 0.0208 to 0.0391, 0.0263 to 0.0407, 0.026 to 0.0476 °C/y respectively for minimum, mean and maximum mean annual temperature. The target station of the Jungfraujoch shows the higher increasing of the mean maximum annual temperature.

Accordingly, to the WMO guidelines the same procedure was applied on the two thirty years periods 1961-1990 and 1991-2022 (Figure 2). We observed always a positive trend, which is higher for maximum temperature, especially in the period 1991-2022. The target site trend rate experiences a high increasing of the minimum annual temperature focused on the period 1991-2022.

The changing points are, in most of the cases, positioned near the 1990 year and confirmed the right choice of splitting the observation period on two thirty-years long periods (Table S1 and Figure S1, Supplementary Materials).

About the question of the Elevation Dependence Warming, considering the 1961-2022 period, it seems that there isn't a clear of highest increasing of the minimum, mean annual temperature with the elevation. About the maximum, focusing on 6 of the 11 sites a linear positive increasing can be seen, but 11 sites are probably few to confirm the significance of this result (Figure S3 Supplementary Materials). Another question is if we considered the two thirty years periods, with a positive increasing of the trend rates for the minimum annual temperature and a negative one for the maximum annual temperature (Figure 3). Those results must be detailed, extending the investigations with a huge number of meteorological stations both in Europe and over the world, the elevation dependence warming is a vital open issue.

3. METHOD

The daily temperature at the target station (TS), the Jungfraujoch, given a backup station (BS), $T_{TS|BS,mod}$, is defined as the sum of three components:

$$T_{TS|BS,mod}(t) = T_{BS,obs}(t) + TLR_{BS,m}(Z_{TS} - Z_{BS}) + \varepsilon_{BS,m}(t) \quad (1)$$

1) $T_{BS,obs}$ is the observed daily temperature at the backup station (BS) (here one of the ten considered in the analysis see Table 1); 2) a deterministic component which is the product of the temperature lapse rate $TLR_{BS,m}$ and the elevation difference between the target and the backup station $(Z_{TS} - Z_{BS})$; 3) $\varepsilon_{BS,m}$ is a random noise which comes from the statistical distribution of the residuals. The subscript "m" refers to the monthly variability of the parameters which is mandatory to follow the seasonality temperature's behavior, while the subscript "mod" means modelled.

Focusing on the period 1961-2022, we selected the 1980-99 period to estimate the model's parameters (Calibration Period) and the others 1961-79 and 2000-2022 to evaluate the performances in the past and in the future (Validation Periods). For each couple of TS and BS, within the calibration period, the TLR parameter was estimated defining a possible range of variability from -1 to +1°C/100 m and calculating the sum of squared errors between observations and simulations. The optimal value of the TLR is that which minimizes the sum of squared errors. The difference between the observed time series and the deterministic component defines the residuals:

$$\varepsilon_{BS,m}(t) = T_{TS,obs}(t) - T_{BS,obs}(t) - TLR_{BS,m}(Z_{TS} - Z_{BS}) \quad (2)$$

For each month, using the Matlab "fitdist" function, with the maximum likelihood method, the parameters of four statistical distributions (Normal, GEV, Stable, TLocationScale) were estimated. Kolmogorov Smirnov and Anderson Darling tests at 5% of significance level were applied to confirm or discard each distribution and theirs lowest values suggested the best. The calibration phase defines 12 values of the TLR and depending of the best statistical distribution, from 24 to 48 parameters for the residual component. To evaluate the model's performances in both calibration and validation periods, four indices of performance were considered, comparing the observed (obs) and modeled temperature (mod): the Pearson coefficient ρ_P, the Spearman's rho ρ_S, the Kendall's tau τ_K, and the root mean square error RMSE. In the next, we provide the formulas to calculate the empirical estimates.

$$\rho_P = \frac{\sum_{t=1}^{n}(T_{TSobs}(t) - \overline{T_{TSobs}})(T_{TS|BSmod}(t) - \overline{T_{TS|BSmod}})}{\sqrt{\sum_{t=1}^{n}[T_{TSobs}(t) - \overline{T_{TSobs}}]^2} \cdot \sqrt{\sum_{t=1}^{n}[T_{TS|BSmod}(t) - \overline{T_{TS|BSmod}}]^2}} \quad (3)$$

$$\rho_S = 1 - 6\frac{\sum_{t=1}^{n} d_t^2}{n(n^2 - 1)} \quad (4)$$

$$\tau_K = \frac{2}{n(n-1)}\sum_{t<j}^{n} sgn(T_{TSobs}(t) - T_{TSobs}(j))sgn\left(T_{TS|BSmod}(t) - T_{TS|BSmod}(j)\right) \quad (5)$$

$$RMSE = \sqrt{\frac{1}{n}\sum_{t=1}^{n}\left[T_{TS,obs}(t) - T_{TS|BS,mod}(t)\right]^2} \quad (6)$$

For each index the symbols meaning are: n the number of days, T_{TSobs} is the daily observed time series, $T_{TS|BSmod}$ is the daily modeled time series related to each couple TS|BS; the overlined symbols such as $\overline{T_{TSobs}}$ defines the mean of the variable within the considered period (Calibration or Validation). About the Spearman's correlation coefficient, d_t^2 is the square of the difference between the rank of the observations and the rank of the estimations at daily scale. Within the Kendall's Tau formula "sgn" is the sign function that return the sign of a real number.

Repeating this procedure for all the 10 meteorological stations, we obtained 10 estimations of the daily temperature time series at the target site, and we calculated the ensemble as the mean of them:

$$T_{TS,Ens}(t) = \frac{1}{m}\sum_{i=1}^{m} T_{BS_i,obs}(t) + TLR_{BS_i,m}\left(Z_{TS} - Z_{BS_i}\right) + \varepsilon_{BS_i,m}(t) \quad (7)$$

The comparison between the observed time series and the "ensemble" one allows to calculate and evaluate the ensemble performances based on the same indices previously defined (Eq.s 3-6). Because some stations started the observations from 1864, we extended the simulation period backward to obtain the daily time series at the Jungfraujoch site from that year. We highlight that the coverage of the observed time series did not allow always to have 10 stations to make the mean, so the ensemble, sometimes is based just on 1 or 2 stations. A further validation of the estimated mean daily temperature time series within the period 1864-1933 was made by the comparison with the one obtained by Imfeld et. al (2023) (https://doi.org/10.1594/PANGAEA.950236). From this last, we selected the closest grid point with the lowest elevation difference compared to the target station position (the elevation was estimated by google earth and its coordinates are: 46.54937 N; 8.005821 E; 3565 m a.s.l).

The reconstruction of the high elevations sites with the TLR method is not a novelty in literature (Rolland 2003, Pepin et al. 2005, Blandford et al. 2008, Minder et al. 2010, Kirchner et al 2012, Petersen et al. 2013, Kattel et al. 2015, Jobst et al. 2017), and gave good results, especially for the mean monthly temperature time series estimation. Improvements of our work are: a statistical model of the residual component, is a pivotal factor to estimate the variability, which can be really different for each season and for each variable (maximum, mean or minimum temperature). A good statistical model, allows, with a Montecarlo method to randomly generate random sample from these distributions defining model's estimation uncertainty and not just their mean values. Moreover, the definition of an "ensemble" simulation which is based on many meteorological stations, makes the estimations much more reliable and less exposed to the harsh meteorological conditions which can damage the specific monitoring sites. With the support of other stations, just with 20 years of overlapping observation period between the target sites and back-up station, models can be calibrated and the temperature time series can be extended at the same observation period length of the back-up station. The simplicity, parsimony, low data requirements, without need of any other

measured variables (relative humidity, wind velocity and direction, meteorological weather pattern, solar radiation, cloud cover) of the proposed method may represent points of a strength.

310

4. RESULTS AND DISCUSSION

Model's performances were compared in both calibration and validation periods, initially for each station and then considering the "Ensemble". Then, the long-term time series at the target site was analyzed.

4.1 Model's parameters: TLR

The temperature lapse rate is the parameter which states the rate at which the air will cool with the elevation. In case of no heat exchanged with the outside system the cooling is adiabatic. This parameter varies from about -0.98°C/100m for dry air (i.e., the dry-air adiabatic lapse rate) to about -0.4°C/100 m (i.e., the saturated adiabatic lapse rate; Dodson and Marks 1997). However, the process is rarely adiabatic and many factors can influence the temporal and spatial variability of it (cloud cover, land cover, wind conditions, weather pattern). An environmental lapse rate of -0.65°C/100 m is a typical value used for its global mean and is commonly used in most of the models which simulate the earth surface processes (hydrological, meteorological, biological).

In Figure 4, the monthly variability of the TLR parameters estimated within the period 1961-2022, comparing the temperature at the target and back-up stations pooling together all the sites are showed.

Our results indicate strong seasonal variability in the median and IQR range, which greater absolute values and lower dispersion in summer months, compared to the less steep values in the winter season. The TLR median values differ between minimum and maximum temperatures. For minimum temperature, the range of monthly median values spans from: -0.54°C/100 m to -0.62°C/100 m, with lower monthly variability, compared to the maximum temperature where the range falls within: -0.48°C/100 m to -0.69°C/100m.

In terms of the IQR range, winter months - January, February, November, and December- experience the high variability from 0.11°C/100 m to 0.15°C/100 m for both maximum and minimum temperatures. These higher values are consistently observed in maximum temperature for each of these months. Conversely, the mean temperature shows lower variability (Table 2).

These results confirm the seasonal variability of the temperature-elevation dependence decreasing and the importance of considering different values for each of the 3 temperature variables (Max, Mean, Min). Particularly our results are comparable with those found in literature from Rolland et al. (2003), Navarro Serrano et al. (2018), which highlighted that the uncertainty of considering the constat environmental lapse rate of -0.65°C/100m is really high and not suitable to reproduce with enough precision the daily temperatures.

The optimal values of the TLR parameters for each station, that will be used for the reconstruction of the long-term time series, was reported in the Table S2 and Figure S4 (Supplementary Materials). These values have been obtained minimizing the sum of squared errors between the observations and the deterministic part of the modeled time series, within each month of the period 1980-1999. About the minimum temperature, the TLR values are more or less the same among 8 of the 10 back-up stations, with values within the range -0.4°C/100 m to -0.7°C/100 m. About the maximum temperature the seasonal shape is much more evident, and the annual excursion is from -0.4°C/100 m to -0.9°C/100m. Steeper values were found in summer and early autumn and lower ones in November and winter months. The mean temperature stays in the middle. Related to all of the three variables the meteorological station of Sonnblick gives the

lowest absolute values and can be considered as an upper bound, especially for maximum temperature and generally for winter months.

The Figure S5 (Supplemetary materials) shows the boxplot of the annual TLR distribution among all of the 10 back-up stations from 1961 to 2022. From these graphs we recognize the high variability which affects the maximum temperature and a sinusoidal trend of the median values especially for maximum and minimum temperatures. Any positive or negative linear trend can be identified even if the median TLR time series cannot be defined as constant.

The choice of the calibration period from 1980-1999 (which was selected independently and without knowing this information) seems appropriate, because the variability in this period can be considered as the same compared to the other 20 years long periods. An exception is the 1981 year about the maximum and mean temperature, with an extreme lower value compared to the other 61 years.

The median values of the TLR seems to have higher values in the last 20 years period 2001-2020 about the maximum temperature.

4.2 Residuals' distributions

Residuals are defined as the difference between the observed daily temperature time series at the target site and the modeled one, using the observations from each of the backup station (Eq.2). Concerning the calibration period, the residuals statistical distribution was fitted for each month and then selected accordingly to the lowest values of the statistical tests (Kolmogorov-Smirnov and Anderson-Darling). A statistical analysis of the residuals is important to define the variability and the uncertainty of the model's estimations. Figure 5 shows for each month and related to the maximum, mean and minimum temperature the kernel density functions mirrored on the vertical axis (violin plot). These distributions come from the pooling of all the daily residuals for all the 10 meteorological stations considered within the calibration period (10 backup stations for 20 years of 365 days).

Frome these graphs we remarked the higher variability of the maximum temperature which shows higher standard deviation values. The mean values are close to 0, which demonstrate that the model isn't affected by a constant over/underestimation. In Table **3**, statistical indexes of mean, standard deviation, skewness and kurtosis coefficients help to summarize better differences among the three variables.

About the distribution's asymmetry we found always positive values (right tailed distributions) with higher values in winter months for minimum temperature. The kurtosis coefficients, pointed out a quasi-normal behavior about the summer residuals of the maximum temperature (values close to 3). All of the kurtosis coefficients are generally higher than 3 which stave off from the normality. Within the supplementary materials, on Table S3, about each station and for each month, the best distribution was reported. Generally,

the Generalized Extreme Value distribution explains better the variability of the winter months, rather than the Stable and T-Location which perform better for summer months.

4.3 Model's performances

The evaluation of model's performances started with the analysis of the results obtained for each of the 10 meteorological stations and then focusing on the ensemble within the calibration period 1980-99 and the validation periods 1961-1980 and 2000-2022.

The calibration period, from 1980-1999 was selected because of two reasons: 1) the changing point analysis of the observed time series reported in section 2 showed that, in most of the cases, close to the year 1990, the mean annual temperature was subjected to the highest increasing; 2) in this way the model can be evaluated in a subsequent period (2000-2022) but mainly also in a previous one (1961-1980). In the

Table **4**, RMSE and Pearson's correlation coefficient were calculated for all the three variables and the 10 stations and at the end about the ensemble. The last two rows of each table show maximum and minimum values among them. In the calibration period the RMSE spans from 2.26°C to 3.32°C, 1.56°C to 2.95°C, and 1.79°C to 3.30°C respectively for maximum, mean and minimum temperatures. High correlation coefficients between modeled and observed time series was found, with values which spans from 0.87 to 0.945, 0.90 to 0.97 and 0.88 to 0.97 always for the same variables in the same order.

Comparable performances, or even slightly better, were obtained in the validation period 1961-1979 about all the three variables. The 2000-2022 validation period shows higher errors about the maximum temperature (from 2.39°C to 3.42°C) but better for mean and minimum temperatures (1.56°C to 2.90°C and 1.72°C to 3.22°C). These results can be partially explained by the analysis of the observed trends which affected differently the observed 10 time series as explained in section 2. In addition, maximum temperature can be also affected by an elevation dependent warming, or accordingly with the Stefan Boltzmann law, the rate of temperature increasing is higher at high temperature due to the nonlinear relationship between the longwave outgoing flux from the earth surface and its temperature.

The validation period 1961-79 experiences an increasing of the mean annual temperature which is generally smaller than that observed in the last 30 years. So, the different trend rates between the Jungfraujoch target site and any of the others backup stations is a source of errors within a single model.

RMSE values are, however, smaller than those found in literature about the same area of the Swiss territory from Pfister and Imfeld in some past works (Pfister et al. 2020, Imfeld et al. 2023).

From Table S4 (Supplementary Materials) we analyzed rank-based correlation coefficients of Spearman and Kendall, which confirmed the model's capability to follow the same trend of the observed variables at the target site even if it can be different from the linearity. Spearman's correlation coefficients span from 0.88 to 0.98 both in the calibration and validation periods. Kendall's tau coefficients span from 0.70 to 0.87 both in calibration and validation periods.

Finally, since our aim is to define a reliable long term time series also in the past, we defined the ensemble as the mean of the ten time series which comes from each couple of back-up/target stations. In this way performances are significantly better especially for the mean temperature: the RMSE and the Pearson

correlation coefficients within the period 1961-2022 are: 2.25, 1.85, 2.14 °C and 0.89,0.92 and 0.91about maximum, mean and minimum temperatures. The high values of the correlation coefficients can be visualized within the Figure 6, which, on the panel left, shows the scatterplot between the observed and modeled time series and we highlight that most of the points stay close to the 1:1 line, visually confirm the performances previously described. The panel right compares the mean daily errorbar always in the period 1961-2022; we can see that the mean daily temperature is really close to the observed one.

Maximum temperatures are affected by higher errors in January, February October and December rather than the minimum which shows higher distances in January, February and October. Slight underestimation was found for all of the three variables during the year.

4.4 Long-term time series reconstruction

The ensemble estimation of the daily temperature time series at the target station from 1864, was obtained as the mean of all the 10 estimations, related to each station. We highlight that the overlapping period of observation among the 10 sites was without lack of data just from 1961 to 2022. For the period 1864-1900 the Col Du Grand Saint Bernard is the only site in which maximum and minimum daily observations are available, After the year 1900 at least 3 stations allow to estimate the temperature at the target site (Figure 7) About the mean temperature, the observation started from 1933, and results showed a good agreement.

The yearly mean of all the estimated time series is pretty close together especially after the 1960 (Figure 7). The observed time series constitutes generally the upper boundary especially in the last 20 years compared to the 10 estimated time-series.

The mean annual temperature at the target site shows stable values from 1864 to 1960, a slight increase from 1960 to 1980 and a significant increase from 1980 to 2022. Is important to highlight that the Col Du Grand Saint Bernard meteorological station, the only available station before 1900, shows high mean values on the maximum temperature with an abrupt positive shift compared to the mean values which come later than the 1900 from the Zugspitze, Sonnblick and Rudolshuette sites. Maximum temperature rises more than mean and minimum ones during the last 60 years.

Finally, Figure 8 shows the estimation of the daily time series at Jungfraujoch from the 1864. Here we reported just the yearly errorbar of the observed time series (red color) and the ensemble simulation (blue color). We highlight on the upper right part of the figure the subdivision on simulation, calibration and validation periods defined in the previous chapters. Each subplot shows the same high performances within the two validation periods about the yearly Minimum and Maximum temperature and an even better results for the mean considering the 1933-1961 subperiod. The amplitude of the errorbar is a visual confirm that also the variability is well reproduced.

4.5 Comparison with the gridded dataset published by Imfeld et al 2023

For a further validation of the long-term mean daily temperature “ensemble” time series, we considered a high-resolution (1km x 1km), daily reconstructions of temperature fields for Switzerland from 1763 to 2020 estimated using the analogous resampling method and subsequent data assimilation (Imfeld et al. 2023).

From this database, the mean daily temperature of the closest grid point (46.54937 N; 8.005821 E; 3565 m a.s.l, 1.6 Km far from the TS station) to the Jungfraujoch station, was selected for a comparison. Observations started from 1933, and we can observe a good agreement in mean annual temperature and errorbars, especially before 1980. Discrepancies slightly increase within the period 1990-2010 while in the period 1864-1932, we found a very good agreement between the "ensemble" and values which come from the work of Imfeld et al. (2023) both for the mean and errorbars. (Figure 8).

Figure 9 compares the ensemble mean daily temperature and the values from Imfeld et al. 2023 within the period 1864-1932. Comparing the ensemble mean daily temperature in the 1864-1932 period, we calculated a root mean square error less than 2 °C and a correlation coefficient higher than 0.9 which is similar to the one between the observed and simulated time series within the period 1961-2022. The ensemble simulation has lower variability especially in January and February and similar one in the rest of the year. As we expected the variance is higher in these months compared to the spring and autumn seasons.

5. CONCLUSIONS

Starting from long time series of daily temperature observations from 10 meteorological stations from ECA&d and Meteo Swiss databases we reconstructed the historical time series at the Jungfraujoch.

A meticulous selection of each site was primarily undertaken, focusing solely on mountain peak stations with elevations higher than 2000 m. In this way we minimize the thermal inversion phenomena. After that we defined a model which estimated the daily temperature at the target site as the sum of the observed temperature at the back-up station plus a deterministic and a stochastic component. The first is the product of the temperature lapse rate and the elevation difference between target and backup station. The second one describes the statistical distribution of the residuals. The temperature lapse rate, with a monthly variability, is estimated minimizing the sum of squared errors within the calibration period 1980-1999. The parameters values are comparable to those found in literature about the same area. Generally steepest values were found in winter about the minimum temperatures and in summer for maximum temperatures. The median values span from -0.48°C/100 m to -0.69°C/100 m considering the pooling of all the stations for the whole observation period 1961-2022. TLR of maximum temperature shows the highest variability. About the residual's distributions, the best one among GEV, Normal, Stable and T-Location was selected accordingly to the minimum values of the statistical tests of Anderson-Darling and Kolmogorov-Smirnov. Extreme value distribution fit well winter months and maximum temperature. About minimum temperature and summer months they experience much more stability.

Analyzing the moments of the residuals, we found always mean monthly values near 0, a generally positive skewness coefficient and a kurtosis coefficient greater than 3, which highlight a slightly greater dispersion than the normal one.

Even if the TLR method isn't new in literature a good study of the residual's component is mandatory to describe the estimation's uncertainty.

Finally, the "ensemble" time series of minimum, mean and maximum temperature at the target site of Jungfraujoch was calculated. This latter allows to increase the model's performances with correlation coefficients higher than 0.9 and RMSE equal to 2.25, 1.85, 2.14 °C respectively for maximum, mean and minimum temperature within the period 1961-2022. Maximum temperature is affected by greater errors and higher variability probably because of the different increasing rates with the elevation, correlated at the climate change.

With the same method, we reconstructed the long-term daily temperature time series at Jungfraujoch since 1864. This latter can be a starting point for a comparison with other atmospheric variables (greenhouse gases, solar radiation, relative humidity) or can be the driver for hydrological or glaciological models.

In addition, it can be compared with other high elevation time series to better understand this unique, poor monitored and harsh environment rich of biodiversity. Future works can arise: the same method could be applied in other mountain chains over the world studying the difference among them (Himalaya, Tibetan plateau, Ande, Rocky Mountains). The strength point of this method consists in its low data requirements because it needs just daily temperature observations without any others measurements of atmospheric variables, which are not generally measured at high elevation sites (relative humidity, solar radiation,

weather pattern). The only requirement is a proper selection of the meteorological stations with consistent and reliable dataset and a rigorous analysis of the residuals. Another improvement can be related to the temporal resolution of dataset. Using hourly resolution probably the calibration period can be reduced and the model can be refined to estimate the diurnal variability.

AUTHOR CONTRIBUTIONS

Marco Bongio performed data analysis and made all the manuscript figures with advice from Riccardo Scotti and Carlo De Michele. The model's code was implemented by Marco Bongio in Matlab. Marco Bongio wrote the manuscript with contributions from all co-authors.

Tables

ST CODE	NAME	Database	Lat.	Long.	Elevation [m]	From	To
VIL	Villacher Alpe	ECA&D	46°36'12''	13°40'23''	2140	1921	2022
ZUG	Zugspitze	ECA&D	47°25'20''	10°59'12''	2964	1901	2022
SON	Sonnblick	ECA&D	47°03'15''	12°57'27''	3109	1886	2022
PAT	Patscherkofel	ECA&D	47°12'32''	11°27'43''	2251	1940	2022
KRE	Kredarica	ECA&D	46°22'43''	13°50'56''	2513	1955	2022
RUD	Rudolfshuette	ECA&D	47°08'00''	12°37'00''	2304	1961	2022
GUE	Gütsch	MeteoSwiss	46°39'00''	8°37'00''	2286	1954	2022
GSB	Col du Grand St. Bernard	MeteoSwiss	45°52'00''	7°10'00''	2472	1864	2022
SAE	Säntis	MeteoSwiss	47°15'00''	9°21'00''	2501	1882	2022
WFJ	Weissfluhjoch	MeteoSwiss	46°50'00''	9°48'00''	2691	1959	2022
JUN	**Jungfraujoch**	**Meteo Swiss**	**46°33'00''**	**7°59'00''**	**3571**	**1933**	**2022**

Table 1. Meteorological stations characteristics.

TLR [°C/Km] PARAMETERS (1961-2022)													
Var	**Index**	**J**	**F**	**M**	**A**	**M**	**J**	**J**	**A**	**S**	**O**	**N**	**D**
T Min	Med	-0.0054	-0.0055	-0.0058	-0.0062	-0.0062	-0.0061	-0.0060	-0.0061	-0.0057	-0.0056	-0.0056	-0.0053
	IQR	0.0012	0.0014	0.0010	0.0010	0.0008	0.0008	0.0009	0.0008	0.0009	0.0010	0.0012	0.0011
T Mean	Med	-0.0051	-0.0053	-0.0057	-0.0061	-0.0062	-0.0064	-0.0065	-0.0066	-0.0060	-0.0056	-0.0054	-0.0051
	IQR	0.0012	0.0012	0.0011	0.0009	0.0009	0.0009	0.0009	0.0009	0.0011	0.0010	0.0011	0.0011
T Max	Med	-0.0048	-0.0051	-0.0054	-0.0059	-0.0060	-0.0064	-0.0068	-0.0069	-0.0062	-0.0057	-0.0052	-0.0049
	IQR	0.0014	0.0015	0.0014	0.0012	0.0014	0.0014	0.0015	0.0014	0.0016	0.0015	0.0012	0.0012

Table 2. Median and interquartile range of the TLR parameter for Minimum, Mean and maximum temperature. Results come from the statistical analysis of the 10 meteorological stations for the whole 1961-2022 period.

RESIDUALS STATISTICAL INDEXES (1980-1999 All Stations)													
Variable	**Index**	**J**	**F**	**M**	**A**	**M**	**J**	**J**	**A**	**S**	**O**	**N**	**D**
T Max	Mean [°C]	0.000	-0.027	0.036	0.023	-0.039	0.015	-0.029	0.014	0.021	-0.020	0.031	-0.020
	Std [°C]	2.966	3.123	2.970	2.717	2.654	2.617	2.580	2.680	2.704	2.719	2.893	2.975
	Skewness	0.567	0.283	0.301	0.269	0.323	0.156	0.329	0.269	0.364	0.346	0.440	0.598
	Kurtosis	4.803	3.719	3.613	3.683	3.677	3.923	3.428	3.410	3.574	3.554	4.110	4.956
T Mean	Mean [°C]	-0.001	-0.024	0.041	-0.003	-0.025	0.012	-0.015	0.001	0.019	-0.003	0.008	-0.009
	Std [°C]	2.520	2.692	2.365	2.237	1.975	1.826	1.707	1.866	2.010	2.251	2.472	2.695
	Skewness	0.673	0.491	0.350	0.597	0.478	0.226	0.238	0.357	0.655	0.635	0.586	0.819
	Kurtosis	4.970	3.918	3.679	4.231	4.827	5.347	3.910	4.460	4.767	4.467	4.449	5.446
T Min	Mean [°C]	-0.002	-0.008	0.028	-0.022	-0.005	0.018	-0.018	-0.005	0.011	0.005	-0.012	0.002
	Std [°C]	2.982	3.161	2.648	2.494	2.152	1.967	1.904	1.994	2.275	2.684	2.808	3.168
	Skewness	0.842	0.649	0.485	0.567	0.383	0.153	0.265	0.406	0.640	0.725	0.600	0.916
	Kurtosis	5.350	4.007	4.124	4.508	5.696	4.583	4.071	5.518	5.079	4.670	4.482	5.413

Table 3. Mean, Standard deviation, Skewness and Kurtosis coefficients of the residual's distributions for each month. These values are obtained considering the pooling of all of the 10 meteorological stations within the calibration period.

T Max - RMSE [°C]			
STATION	**1961-1979**	**1980-1999**	**2000-2022**
VIL	3.082	3.274	3.319
ZUG	2.408	2.730	2.585
SON	2.839	3.121	3.162
PAT	2.855	2.958	3.051
GUE	2.325	2.410	2.407
GSB	2.223	2.256	2.409
SAE	2.240	2.332	2.392
WFJ	2.189	2.421	2.425
KRE	3.078	3.317	3.424
RUD	3.108	3.197	3.195
Max	**3.108**	**3.317**	**3.424**
Min	**2.189**	**2.256**	**2.392**

T Max - r_P			
STATION	**1961-1979**	**1980-1999**	**2000-2022**
VIL	0.883	0.870	0.875
ZUG	0.932	0.914	0.931
SON	0.899	0.880	0.885
PAT	0.908	0.899	0.903
GUE	0.935	0.935	0.940
GSB	0.943	0.939	0.940
SAE	0.945	0.937	0.943
WFJ	0.939	0.933	0.941
KRE	0.890	0.875	0.879
RUD	0.895	0.880	0.889
Max	**0.945**	**0.939**	**0.943**
Min	**0.883**	**0.870**	**0.875**

T Mean - RMSE [°C]			
STATION	**1961-1979**	**1980-1999**	**2000-2022**
VIL	2.995	2.946	2.899
ZUG	1.841	1.886	1.999
SON	2.785	2.807	2.782
PAT	2.521	2.489	2.520
GUE	1.773	1.561	1.556
GSB	1.958	1.686	1.680
SAE	1.751	1.714	1.699
WFJ	1.630	1.596	1.621
KRE	2.730	2.746	2.765
RUD	2.883	2.756	2.735
Max	**2.995**	**2.946**	**2.899**
Min	**1.630**	**1.561**	**1.556**

T Mean - r_P			
STATION	1961-1979	1980-1999	2000-2022
VIL	0.894	0.897	0.903
ZUG	0.961	0.959	0.956
SON	0.909	0.906	0.910
PAT	0.926	0.929	0.931
GUE	0.964	0.971	0.973
GSB	0.956	0.966	0.969
SAE	0.966	0.966	0.968
WFJ	0.972	0.972	0.973
KRE	0.919	0.921	0.924
RUD	0.907	0.913	0.918
Max	**0.972**	**0.972**	**0.973**
Min	**0.894**	**0.897**	**0.903**

T Min – RMSE [°C]			
STATION	**1961-1979**	**1980-1999**	**2000-2022**
VIL	3.055	3.296	3.209
ZUG	2.133	2.551	2.422
SON	2.760	3.127	3.075
PAT	2.448	2.766	2.754
GUE	2.055	1.794	1.721
GSB	2.143	1.877	1.777
SAE	2.032	1.887	1.867

T Min - r_P			
STATION	**1961-1979**	**1980-1999**	**2000-2022**
VIL	0.900	0.884	0.891
ZUG	0.953	0.938	0.947
SON	0.922	0.896	0.900
PAT	0.937	0.921	0.924
GUE	0.955	0.964	0.968
GSB	0.952	0.961	0.967
SAE	0.959	0.962	0.964

WFJ	1.890	1.821	1.783
KRE	3.031	3.249	3.226
RUD	2.900	3.179	3.099
Max	**3.055**	**3.296**	**3.226**
Min	**1.890**	**1.794**	**1.721**

WFJ	0.960	0.966	0.968
KRE	0.905	0.890	0.893
RUD	0.913	0.898	0.906
Max	**0.960**	**0.966**	**0.968**
Min	**0.900**	**0.884**	**0.891**

Ensemble Performances				
	RMSE [°C]	r_P	ρ_{Sp}	τ_k
T Max	2.247	0.946	0.941	0.800
T Mean	1.852	0.965	0.961	0.840
T Min	2.142	0.956	0.952	0.822

15 Table 4. Model's performances evaluation within the calibration period 1980-99 and the validation periods (1961-79 and 2000-2022). RMSE and Pearson correlation coefficients were reported with the 10 backup stations and for the ensemble simulation.

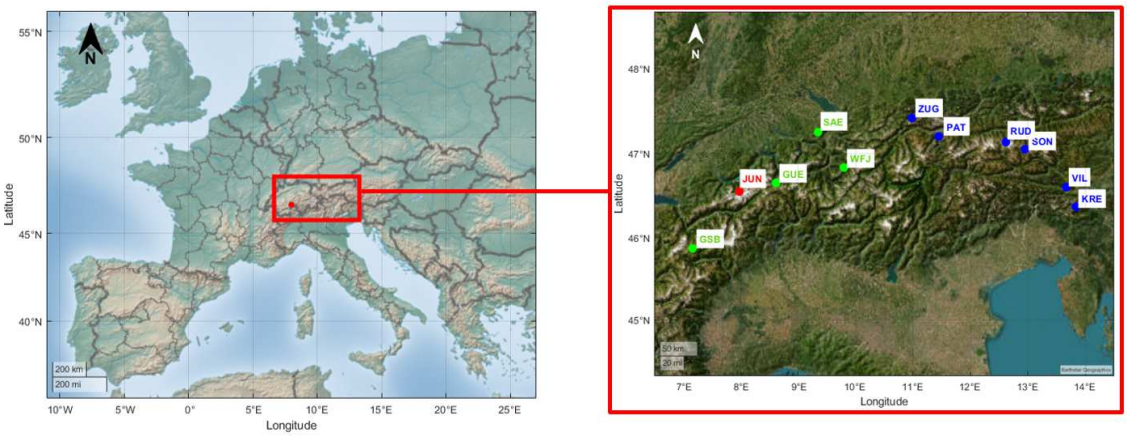

Figure 1. **Panel Left**: Case study Area. **Panel Rigth**: Locations and ID of the 5 meteorological stations from Meteo Swiss database (green and red dots), and 6 from ECA&d (blue dots).

20

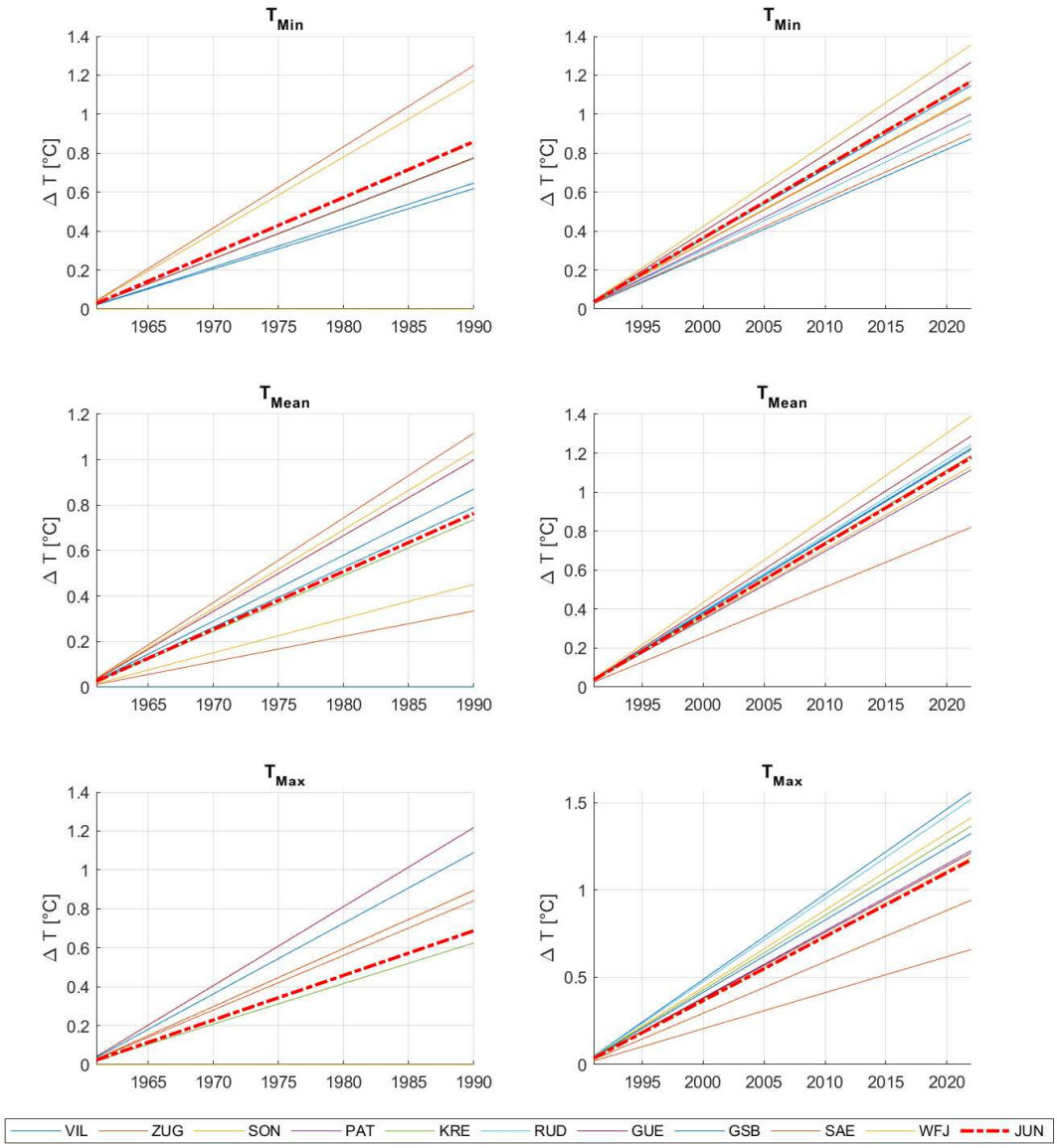

Figure 2. Mean annual temperature analysis of observations: Trend comparison among the 11 meteorological stations considered. (Just significative trends and time series with less than 5% of No data were plotted)

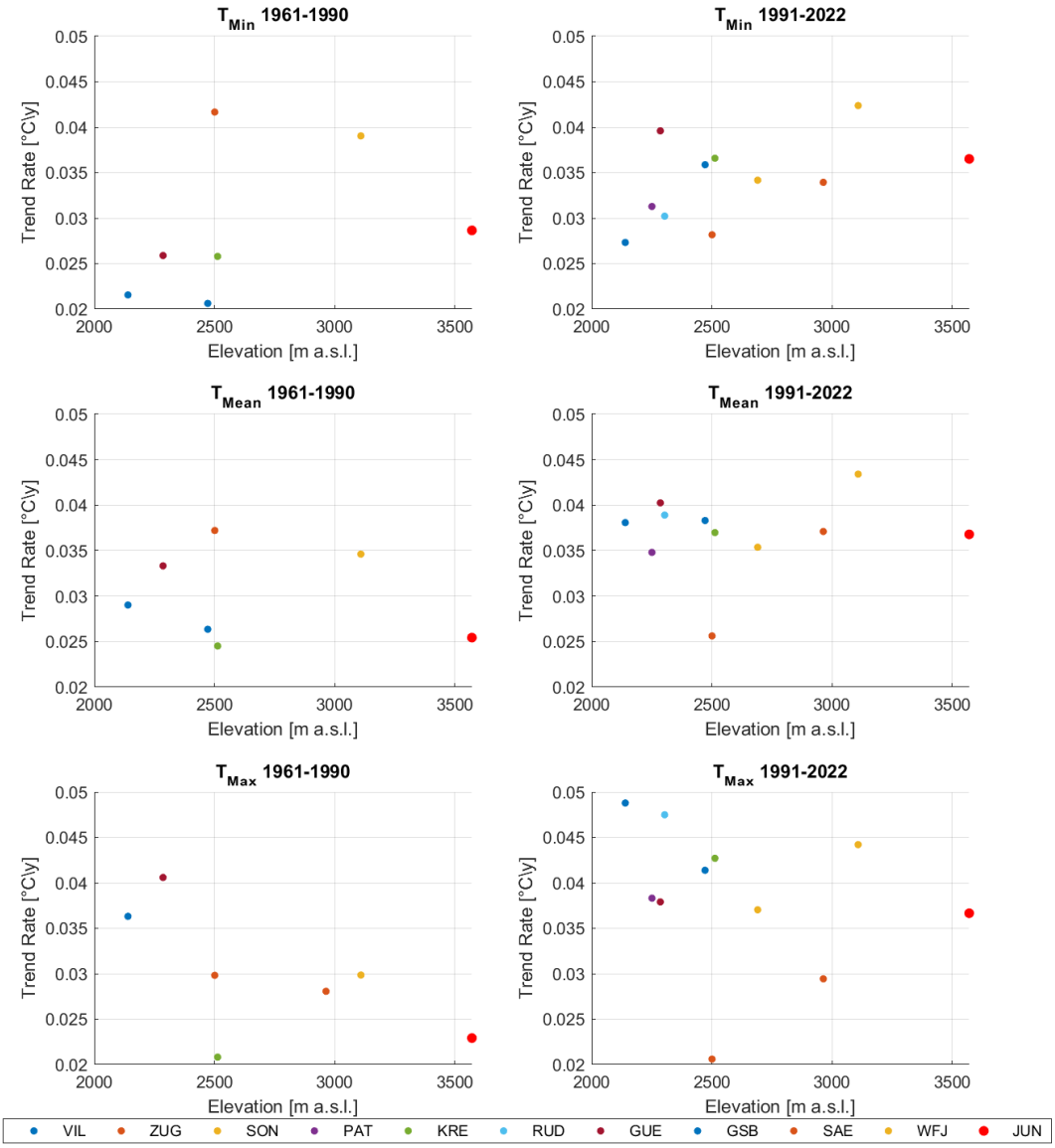

Figure 3. Trend Analysis of the mean annual temperature observed time series against the meteorological stations' elevations. Even if 10 meteorological stations are few to fit a trend it seems that there is a positive EDW for minimum annual temperature and a negative one for maximum annual temperature within the period 1991-2022.

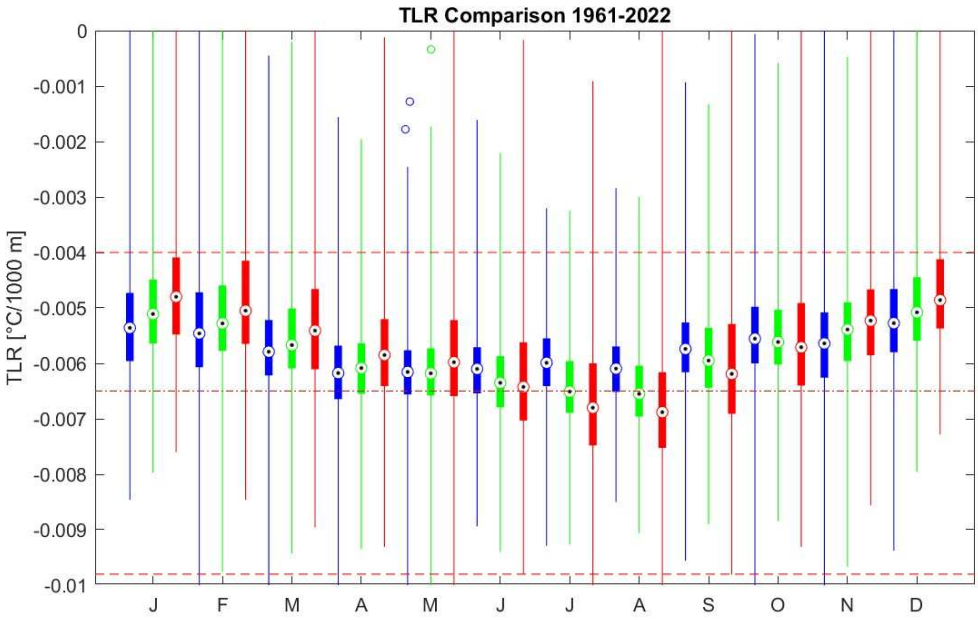

Figure 4. TLR boxplot monthly comparison for maximum (red), mean (green) and minimum (blue), temperature within the period 1961-2022 for all of the meteorological stations. Red Dashed lines indicate the wet and dry adiabatic temperature lapse rate (-0.4 and -0.98°C/100m). Red Dots dashed line shows the Environmental Lapse Rate of -0.65°/100m.

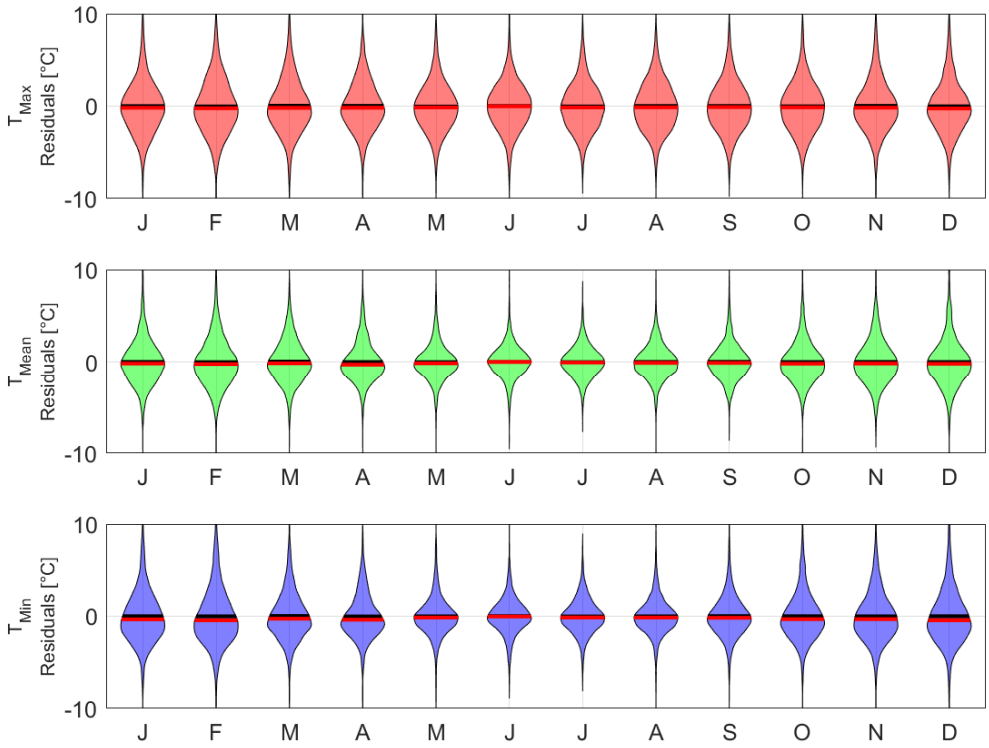

Figure 5. Violin plot of the residual's distributions related to the maximum minimum and mean temperature obtained by the pooling of the 10 stations within the calibration period. Statistical indexes of these distributions are reported in the

Table 3.

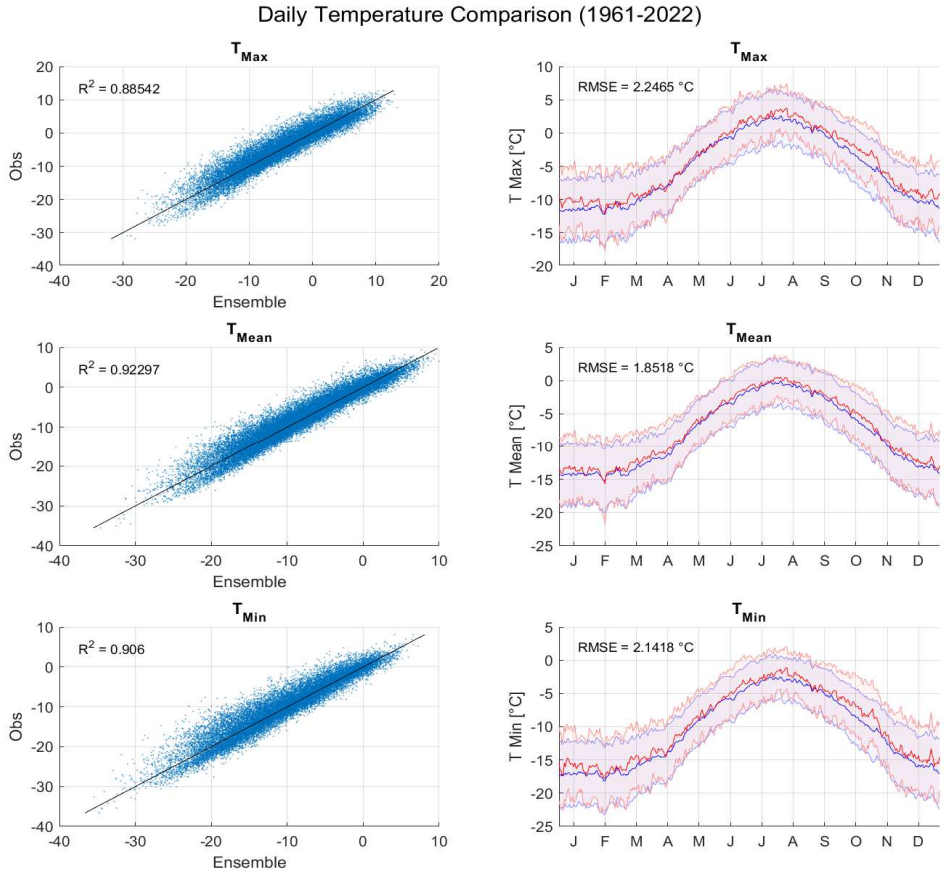

Figure 6. **Panel left**: Scatterplot between ensemble simulation and daily temperature observations. **Panel rigth**: Comparison between daily mean ensemble simulations and observations error bar. Graphs show the period 1961-2022 about the Jungfraujoch target station.

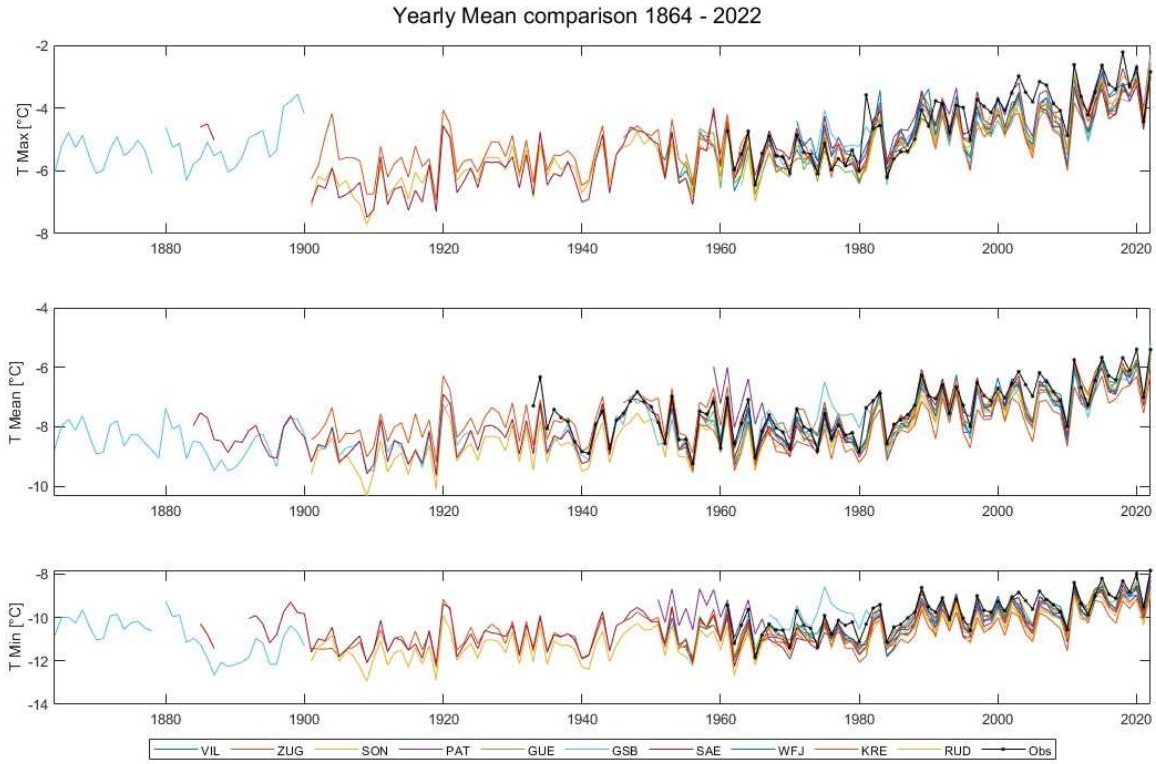

Figure 7. Comparison of the mean annual temperature time series estimations at the Jungfraujoch from 1864. Colored lines represents the different back-up station, with black dotted-line represents the observed time series at Jungfraujoch.

50

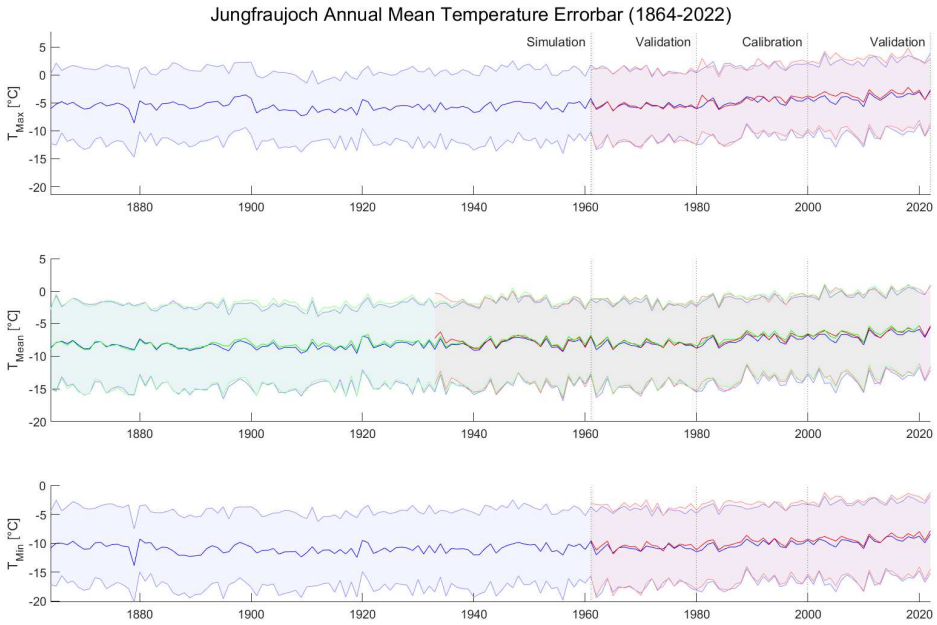

Figure 8. Errorbar of the annual maximum, mean, and minimum time series at the Jungfraujoch target site from 1864 to 2022.With blue lines the “ensemble”, with red lines the observed time series. The green line shows the long-term series estimated by Imfeld et al. 2023.

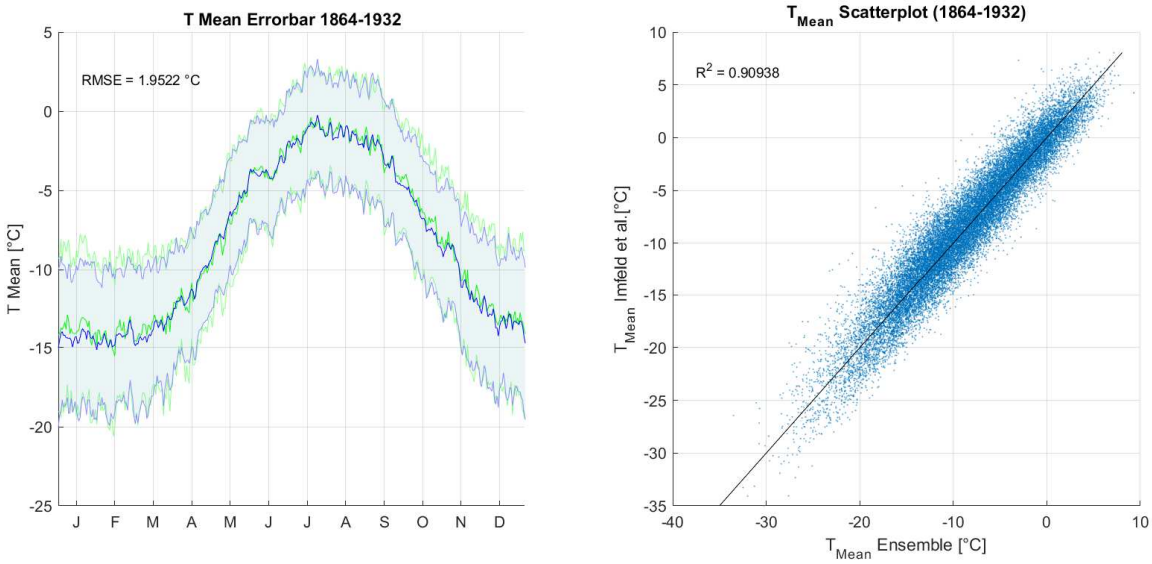

Figure 9. Comparison between the ensemble mean daily temperature (blue line) and the results from Imfeld et al. 2023 reconstruction (green line) within the period 1864-1932. **Panel Left**: Daily Errorbar. **Panel Rigth**: Scatterplot.

Supplementary material

Tables

T Max									
			1961-2022		1961-1990		1991-2022		
ST Name	Elev. [m a.s.l.]	No Data [%]	Trend [°C\Y]	P Value	Trend [°C\Y]	P Value	Trend [°C\Y]	P Value	CP Year
VIL	2140	0.0%	0.0454	6.54E-35	0.0363	9.85E-08	0.0488	4.61E-12	1988
ZUG	2964	0.0%	0.0335	1.54E-25	0.0281	1.82E-04	0.0294	7.76E-08	1987
SON	3109	0.0%	0.0406	6.82E-36	0.0299	1.47E-07	0.0442	4.14E-13	1988
PAT	2251	0.0%	0.0261	9.33E-10	-0.0167	1.74E-01	0.0383	1.56E-09	1988
KRE	2513	0.1%	0.0333	1.00E-25	0.0208	1.22E-04	0.0427	2.80E-09	1988
RUD	2304	11.8%	0.0447	3.02E-36	0.0346	4.58E-08	0.0475	1.34E-12	1989
GUE	2286	0.1%	0.0399	8.18E-27	0.0406	7.23E-06	0.0379	9.98E-09	1987
GSB	2472	6.2%	0.0252	1.00E-18	0.0146	1.44E-02	0.0414	3.68E-10	2013
SAE	2501	0.0%	0.0303	6.27E-23	0.0298	2.61E-05	0.0206	1.86E-04	1987
WFJ	2691	16.3%	0.0190	2.74E-09	-0.0113	1.60E-01	0.0370	2.26E-08	2013
JUN	3571	0.0%	0.0476	7.28E-30	0.0229	7.66E-04	0.0367	4.45E-10	1990

T Mean									
			1961-2022		1961-1990		1991-2022		
ST Name	Elev. [m a.s.l.]	No Data [%]	Trend [°C\Y]	P Value	Trend [°C\Y]	P Value	Trend [°C\Y]	P Value	CP Year
VIL	2140	0.0%	0.0407	3.29E-35	0.0290	9.86E-07	0.0381	3.34E-12	1988
ZUG	2964	0.0%	0.0297	3.37E-23	0.0112	5.23E-02	0.0371	2.18E-10	1988
SON	3109	0.0%	0.0399	1.29E-39	0.0346	8.74E-11	0.0434	1.72E-13	1988
PAT	2251	0.0%	0.0263	1.35E-11	-0.0107	3.19E-01	0.0348	2.36E-09	1988
KRE	2513	0.2%	0.0351	2.42E-30	0.0245	2.32E-05	0.0370	2.32E-10	1988
RUD	2304	11.8%	0.0360	1.70E-33	0.0266	1.19E-06	0.0389	6.31E-12	1988
GUE	2286	0.1%	0.0398	7.39E-31	0.0333	5.11E-06	0.0402	1.10E-10	1987
GSB	2472	0.0%	0.0263	4.14E-22	0.0264	2.22E-05	0.0383	4.51E-10	2013
SAE	2501	0.0%	0.0369	5.91E-27	0.0372	2.68E-06	0.0256	2.40E-06	1987
WFJ	2691	0.1%	0.0328	3.08E-24	0.0151	1.51E-02	0.0354	9.13E-09	1988
JUN	3571	0.0%	0.0376	2.26E-28	0.0254	3.09E-04	0.0368	4.79E-10	1988

T Min									
			1961-2022		1961-1990		1991-2022		
ST Name	Elev. [m a.s.l.]	No Data [%]	Trend [°C\Y]	P Value	Trend [°C\Y]	P Value	Trend [°C\Y]	P Value	CP Year
VIL	2140	0.0%	0.0357	8.90E-32	0.0216	6.65E-05	0.0273	4.93E-11	1989
ZUG	2964	0.0%	0.0238	3.40E-17	-0.0023	6.81E-01	0.0339	2.93E-10	1990
SON	3109	0.0%	0.0391	4.34E-40	0.0390	8.94E-13	0.0424	5.11E-13	1988

PAT	2251	0.0%	0.0263	1.16E-13	-0.0045	6.29E-01	0.0313	5.44E-09	1988
KRE	2513	0.3%	0.0381	7.16E-33	0.0258	1.78E-05	0.0366	5.44E-12	1987
RUD	2304	11.8%	0.0277	1.28E-27	0.0196	2.30E-04	0.0302	2.97E-10	1988
GUE	2286	0.1%	0.0382	6.74E-29	0.0259	3.20E-04	0.0396	2.18E-11	1987
GSB	2472	0.1%	0.0208	3.90E-13	0.0206	1.40E-02	0.0359	1.26E-09	2013
SAE	2501	0.0%	0.0389	3.60E-32	0.0417	2.50E-09	0.0282	1.10E-07	1987
WFJ	2691	16.3%	0.0217	3.54E-10	-0.0214	7.24E-03	0.0342	2.10E-08	1989
JUN	3571	0.0%	0.0345	3.82E-29	0.0287	6.80E-06	0.0365	1.40E-09	1987

Table S1. Preliminary Analysis of the observed time series: Trend of the 5 years moving average of the Yearly minimum, mean and maximum temperature within the period 1961-2022,1961-1990 and 1991-2022 and the p values of the hypothesis test of linear model against a constat model. The last column shows the detection of the changing point.

TLR [°C/Km] OPTIMAL VALUES WITHIN CALIBRATION PERIOD 1980-1999												
	T Max											
	J	F	M	A	M	J	J	A	S	O	N	D
GSB	-0.0051	-0.0053	-0.0059	-0.0060	-0.0061	-0.0072	-0.0081	-0.0081	-0.0071	-0.0057	-0.0051	-0.0051
GUE	-0.0053	-0.0054	-0.0057	-0.0056	-0.0060	-0.0070	-0.0078	-0.0080	-0.0075	-0.0067	-0.0056	-0.0053
KRE	-0.0056	-0.0052	-0.0057	-0.0059	-0.0056	-0.0062	-0.0065	-0.0066	-0.0063	-0.0060	-0.0056	-0.0051
PAT	-0.0052	-0.0050	-0.0057	-0.0058	-0.0063	-0.0069	-0.0071	-0.0071	-0.0065	-0.0059	-0.0051	-0.0047
RUD	-0.0051	-0.0050	-0.0058	-0.0062	-0.0063	-0.0063	-0.0065	-0.0066	-0.0063	-0.0059	-0.0050	-0.0046
SAE	-0.0058	-0.0056	-0.0058	-0.0058	-0.0058	-0.0056	-0.0058	-0.0060	-0.0060	-0.0062	-0.0056	-0.0055
SON	-0.0018	-0.0017	-0.0030	-0.0051	-0.0050	-0.0057	-0.0057	-0.0055	-0.0042	-0.0034	-0.0027	-0.0011
VIL	-0.0047	-0.0047	-0.0054	-0.0059	-0.0060	-0.0067	-0.0066	-0.0065	-0.0059	-0.0053	-0.0048	-0.0044
WFJ	-0.0055	-0.0053	-0.0056	-0.0058	-0.0063	-0.0067	-0.0080	-0.0084	-0.0077	-0.0072	-0.0056	-0.0052
ZUG	-0.0043	-0.0042	-0.0047	-0.0060	-0.0063	-0.0058	-0.0056	-0.0059	-0.0055	-0.0056	-0.0043	-0.0039
	T Mean											
	J	F	M	A	M	J	J	A	S	O	N	D
GSB	-0.0053	-0.0056	-0.0061	-0.0063	-0.0062	-0.0069	-0.0074	-0.0074	-0.0066	-0.0057	-0.0053	-0.0052
GUE	-0.0055	-0.0055	-0.0059	-0.0059	-0.0059	-0.0063	-0.0066	-0.0066	-0.0062	-0.0058	-0.0055	-0.0054
KRE	-0.0056	-0.0051	-0.0057	-0.0060	-0.0059	-0.0064	-0.0063	-0.0064	-0.0061	-0.0058	-0.0054	-0.0051
PAT	-0.0054	-0.0052	-0.0059	-0.0061	-0.0064	-0.0066	-0.0067	-0.0068	-0.0063	-0.0058	-0.0052	-0.0049
RUD	-0.0051	-0.0049	-0.0057	-0.0061	-0.0062	-0.0062	-0.0062	-0.0064	-0.0061	-0.0057	-0.0049	-0.0046
SAE	-0.0059	-0.0056	-0.0059	-0.0060	-0.0060	-0.0058	-0.0058	-0.0059	-0.0058	-0.0059	-0.0056	-0.0054
SON	-0.0031	-0.0027	-0.0042	-0.0060	-0.0061	-0.0065	-0.0062	-0.0061	-0.0051	-0.0043	-0.0037	-0.0022
VIL	-0.0050	-0.0049	-0.0057	-0.0062	-0.0063	-0.0067	-0.0065	-0.0065	-0.0060	-0.0054	-0.0051	-0.0047
WFJ	-0.0057	-0.0054	-0.0058	-0.0059	-0.0062	-0.0062	-0.0065	-0.0067	-0.0063	-0.0061	-0.0055	-0.0053
ZUG	-0.0045	-0.0040	-0.0046	-0.0053	-0.0056	-0.0053	-0.0049	-0.0051	-0.0049	-0.0050	-0.0041	-0.0038
	T Min											
	J	F	M	A	M	J	J	A	S	O	N	D
GSB	-0.0055	-0.0057	-0.0061	-0.0063	-0.0062	-0.0066	-0.0066	-0.0068	-0.0063	-0.0058	-0.0056	-0.0054
GUE	-0.0055	-0.0055	-0.0059	-0.0059	-0.0058	-0.0059	-0.0059	-0.0059	-0.0058	-0.0056	-0.0054	-0.0054
KRE	-0.0056	-0.0053	-0.0059	-0.0061	-0.0062	-0.0066	-0.0062	-0.0063	-0.0061	-0.0058	-0.0057	-0.0052
PAT	-0.0056	-0.0054	-0.0060	-0.0061	-0.0062	-0.0062	-0.0061	-0.0062	-0.0059	-0.0057	-0.0054	-0.0052
RUD	-0.0049	-0.0047	-0.0055	-0.0058	-0.0059	-0.0058	-0.0056	-0.0059	-0.0057	-0.0055	-0.0050	-0.0047
SAE	-0.0060	-0.0058	-0.0061	-0.0061	-0.0062	-0.0059	-0.0058	-0.0058	-0.0058	-0.0060	-0.0057	-0.0056
SON	-0.0043	-0.0037	-0.0051	-0.0063	-0.0064	-0.0068	-0.0060	-0.0058	-0.0057	-0.0054	-0.0048	-0.0035
VIL	-0.0053	-0.0052	-0.0058	-0.0062	-0.0062	-0.0065	-0.0062	-0.0062	-0.0060	-0.0055	-0.0053	-0.0050
WFJ	-0.0058	-0.0055	-0.0058	-0.0060	-0.0061	-0.0061	-0.0059	-0.0060	-0.0060	-0.0060	-0.0056	-0.0054
ZUG	-0.0047	-0.0043	-0.0048	-0.0053	-0.0055	-0.0053	-0.0048	-0.0049	-0.0049	-0.0050	-0.0045	-0.0040

Table S2. Optimal values of the TLR parameters within the period 1980-99, about all the 10 back-up stations, for each month and the three considered variables.

RESIDUALS STATISTICAL DISTRIBUTIONS (1980-1999 All Stations)													
Var	**ST. ID**	**J**	**F**	**M**	**A**	**M**	**J**	**J**	**A**	**S**	**O**	**N**	**D**
T Max	GSB	Stable	Gev	Stable	Gev	T Loc	Stable	Gev	Gev	T Loc	Stable	Gev	Stable
	GUE	Gev	Gev	Stable	Stable	T Loc	T Loc	Stable	Gev	Gev	Stable	T Loc	Stable
	KRE	Stable	Gev	Gev	T Loc	Gev	Stable	Stable	Gev	T Loc	Gev	Stable	Stable
	PAT	Stable	Gev	Gev	Gev	Gev	T Loc	Gev	Stable	Stable	Gev	Gev	Stable
	RUD	T Loc	Gev	Gev	Gev	Stable	Stable	Stable	Gev	Stable	Gev	Gev	Gev
	SAE	Norm	T Loc	Stable	Stable	T Loc	T Loc	T Loc	T Loc	T Loc	T Loc	T Loc	T Loc
	SON	Stable	Gev	T Loc	Gev	Stable	T Loc	Gev	Stable	Stable	T Loc	T Loc	Stable
	VIL	Stable	Gev	T Loc	T Loc	T Loc	Stable	Stable	Gev	Stable	Gev	Gev	Gev
	WFJ	T Loc	Gev	Stable	Stable	Stable	T Loc	Stable	Stable	Stable	T Loc	T Loc	T Loc
	ZUG	T Loc	Stable	Stable	T Loc	T Loc	T Loc	T Loc	Gev	T Loc	Norm	Stable	T Loc
	Prev.	Stable	Gev	Stable	Gev	T Loc	T Loc	Stable	Gev	Stable	Gev	Gev/T Loc	Stable
Var	**ST. ID**	**J**	**F**	**M**	**A**	**M**	**J**	**J**	**A**	**S**	**O**	**N**	**D**
T Mean	GSB	Gev	Gev	Stable	Stable	T Loc	Norm	T Loc	Norm	T Loc	Stable	Stable	Stable
	GUE	Gev	Gev	Stable	Stable	Stable	T Loc	Stable	Gev	Stable	Stable	Gev	Gev
	KRE	Gev	Stable	Gev	Stable	Stable	T Loc	Gev	Stable	Stable	Stable	Stable	Stable
	PAT	Stable	Gev	Gev	Gev	Stable	Stable	Stable	Stable	Stable	Gev	Gev	Stable
	RUD	Stable	Gev	Gev	Gev	T Loc	Stable	T Loc	Gev	Stable	Gev	Gev	Stable
	SAE	T Loc	T Loc	Gev	Stable	T Loc	T Loc	T Loc	T Loc	T Loc	T Loc	T Loc	T Loc
	SON	Stable	Gev	Gev	Gev	Stable	Stable	Gev	Stable	Gev	Gev	Gev	Stable
	VIL	Gev	Gev	Gev	Gev	T Loc	T Loc	Gev	Stable	Gev	Gev	Gev	Stable
	WFJ	Stable	Stable	Gev	Stable	Stable	Stable	T Loc	Stable	T Loc	T Loc	Stable	Stable
	ZUG	T Loc	T Loc	Stable	Stable	T Loc	T Loc	T Loc	Stable	T Loc	Stable	T Loc	T Loc
	Prev.	Gev	Gev	Gev	Stable	Stable/T Loc	T Loc	T Loc	Stable	Stable/T Loc	Stable/Gev	Gev	Stable
Var	**ST. ID**	**J**	**F**	**M**	**A**	**M**	**J**	**J**	**A**	**S**	**O**	**N**	**D**
T Min	GSB	Norm	Stable	Stable	Stable	T Loc	T Loc	Stable	Stable	T Loc	T Loc	Gev	T Loc
	GUE	Gev	Gev	Gev	Gev	Stable	T Loc	T Loc	Stable	T Loc	Gev	Gev	Gev
	KRE	Gev	Gev	Stable	Stable	T Loc	T Loc	Gev	T Loc	Stable	Gev	Stable	Stable
	PAT	Stable	Gev	Gev	Stable	Stable	T Loc	Stable	T Loc	Stable	Gev	Gev	Stable
	RUD	Stable	Gev	Gev	Stable	Stable	T Loc	Gev	T Loc	Stable	Stable	Stable	Stable
	SAE	Gev	Stable	Gev	Gev	Stable	T Loc	T Loc	T Loc	T Loc	Stable	Gev	Stable
	SON	Gev	Gev	Gev	Stable	Stable	T Loc	Stable	Stable	Stable	Stable	Stable	Stable
	VIL	Stable	Gev	Stable	T Loc	T Loc	T Loc	Gev	T Loc	Stable	Gev	Gev	Stable
	WFJ	Gev	Stable	Gev	Stable	Stable	T Loc	Stable	T Loc	T Loc	Stable	Gev	Gev
	ZUG	Stable	Stable	Stable	Stable	Stable	Stable	Stable	Stable	Stable	Stable	Stable	Stable
	Prev.	Gev	Gev	Gev	Stable	Stable	T Loc	Stable	T Loc	T Loc/Stable	Stable	Gev	Stable

Table S3. Statistical Distributions of the residuals for each station for each month. The selection was based on the minimum values of the statistical tests of Kolmogorov Smirnov and Anderson Darling tests. On the last row for each variable the prevailing distribution was selected for each month.

T Max – RMSE [°C]			
STATION	**1961-1979**	**1980-1999**	**2000-2022**
VIL	3.082	3.274	3.319
ZUG	2.408	2.730	2.585
SON	2.839	3.121	3.162
PAT	2.855	2.958	3.051
GUE	2.325	2.410	2.407
GSB	2.223	2.256	2.409
SAE	2.240	2.332	2.392
WFJ	2.189	2.421	2.425
KRE	3.078	3.317	3.424
RUD	3.108	3.197	3.195
Max	3.108	3.317	3.424
Min	2.189	2.256	2.392

T Max - r_P			
STATION	**1961-1979**	**1980-1999**	**2000-2022**
VIL	0.883	0.870	0.875
ZUG	0.932	0.914	0.931
SON	0.899	0.880	0.885
PAT	0.908	0.899	0.903
GUE	0.935	0.935	0.940
GSB	0.943	0.939	0.940
SAE	0.945	0.937	0.943
WFJ	0.939	0.933	0.941
KRE	0.890	0.875	0.879
RUD	0.895	0.880	0.889
Max	0.945	0.939	0.943
Min	0.883	0.870	0.875

T Mean - RMSE [°C]			
STATION	**1961-1979**	**1980-1999**	**2000-2022**
VIL	2.995	2.946	2.899
ZUG	1.841	1.886	1.999
SON	2.785	2.807	2.782
PAT	2.521	2.489	2.520
GUE	1.773	1.561	1.556
GSB	1.958	1.686	1.680
SAE	1.751	1.714	1.699
WFJ	1.630	1.596	1.621
KRE	2.730	2.746	2.765
RUD	2.883	2.756	2.735
Max	2.995	2.946	2.899
Min	1.630	1.561	1.556

T Mean - r_P			
STATION	1961-1979	1980-1999	2000-2022
VIL	0.894	0.897	0.903
ZUG	0.961	0.959	0.956
SON	0.909	0.906	0.910
PAT	0.926	0.929	0.931
GUE	0.964	0.971	0.973
GSB	0.956	0.966	0.969
SAE	0.966	0.966	0.968
WFJ	0.972	0.972	0.973
KRE	0.919	0.921	0.924
RUD	0.907	0.913	0.918
Max	0.972	0.972	0.973
Min	0.894	0.897	0.903

T Min - RMSE [°C]			
STATION	**1961-1979**	**1980-1999**	**2000-2022**
VIL	3.055	3.296	3.209
ZUG	2.133	2.551	2.422
SON	2.760	3.127	3.075
PAT	2.448	2.766	2.754
GUE	2.055	1.794	1.721
GSB	2.143	1.877	1.777
SAE	2.032	1.887	1.867
WFJ	1.890	1.821	1.783
KRE	3.031	3.249	3.226

T Min - r_P			
STATION	**1961-1979**	**1980-1999**	**2000-2022**
VIL	0.900	0.884	0.891
ZUG	0.953	0.938	0.947
SON	0.922	0.896	0.900
PAT	0.937	0.921	0.924
GUE	0.955	0.964	0.968
GSB	0.952	0.961	0.967
SAE	0.959	0.962	0.964
WFJ	0.960	0.966	0.968
KRE	0.905	0.890	0.893

RUD	2.900	3.179	3.099	RUD	0.913	0.898	0.906
Max	**3.055**	**3.296**	**3.226**	**Max**	**0.960**	**0.966**	**0.968**
Min	**1.890**	**1.794**	**1.721**	**Min**	**0.900**	**0.884**	**0.891**

T Max - ρ_{Sp}				**T Max - τ_k**			
STATION	**1961-1979**	**1980-1999**	**2000-2022**	STATION	1961-1979	1980-1999	2000-2022
VIL	0.894	0.884	0.884	VIL	0.716	0.698	0.700
ZUG	0.935	0.917	0.933	ZUG	0.782	0.750	0.777
SON	0.908	0.892	0.897	SON	0.736	0.713	0.719
PAT	0.913	0.906	0.908	PAT	0.744	0.733	0.736
GUE	0.935	0.938	0.942	GUE	0.782	0.784	0.793
GSB	0.944	0.940	0.941	GSB	0.795	0.790	0.791
SAE	0.950	0.939	0.946	SAE	0.806	0.787	0.800
WFJ	0.941	0.937	0.945	WFJ	0.791	0.784	0.798
KRE	0.900	0.888	0.889	KRE	0.725	0.706	0.707
RUD	0.902	0.884	0.893	RUD	0.729	0.704	0.716
Max	**0.950**	**0.940**	**0.946**	**Max**	**0.806**	**0.790**	**0.800**
Min	**0.894**	**0.884**	**0.884**	**Min**	**0.716**	**0.698**	**0.700**

T Mean - ρ_{Sp}				**T Mean - τ_k**			
STATION	**1961-1979**	**1980-1999**	**2000-2022**	STATION	1961-1979	1980-1999	2000-2022
VIL	0.905	0.911	0.913	VIL	0.731	0.736	0.741
ZUG	0.962	0.961	0.958	ZUG	0.835	0.833	0.824
SON	0.915	0.914	0.919	SON	0.747	0.745	0.751
PAT	0.934	0.937	0.937	PAT	0.777	0.782	0.783
GUE	0.969	0.974	0.976	GUE	0.850	0.863	0.868
GSB	0.960	0.968	0.972	GSB	0.828	0.850	0.858
SAE	0.970	0.968	0.971	SAE	0.851	0.848	0.855
WFJ	0.975	0.975	0.977	WFJ	0.866	0.867	0.870
KRE	0.926	0.930	0.931	KRE	0.768	0.774	0.774
RUD	0.915	0.921	0.926	RUD	0.746	0.755	0.763
Max	**0.975**	**0.975**	**0.977**	**Max**	**0.866**	**0.867**	**0.870**
Min	**0.905**	**0.911**	**0.913**	**Min**	**0.731**	**0.736**	**0.741**

T Min - ρ_{Sp}				**T Min - τ_k**			
STATION	**1961-1979**	**1980-1999**	**2000-2022**	STATION	1961-1979	1980-1999	2000-2022
VIL	0.909	0.897	0.901	VIL	0.741	0.719	0.726
ZUG	0.953	0.939	0.948	ZUG	0.818	0.793	0.807
SON	0.925	0.901	0.906	SON	0.769	0.729	0.735

PAT	0.943	0.930	0.932	PAT	0.796	0.772	0.777
GUE	0.960	0.967	0.971	GUE	0.828	0.845	0.856
GSB	0.955	0.963	0.970	GSB	0.819	0.838	0.854
SAE	0.962	0.963	0.966	SAE	0.834	0.838	0.843
WFJ	0.962	0.967	0.971	WFJ	0.839	0.850	0.857
KRE	0.911	0.900	0.902	KRE	0.745	0.725	0.728
RUD	0.919	0.908	0.915	RUD	0.758	0.738	0.750
Max	**0.962**	**0.967**	**0.971**	**Max**	**0.839**	**0.850**	**0.857**
Min	**0.909**	**0.897**	**0.901**	**Min**	**0.741**	**0.719**	**0.726**

Ensamble Performances				
	RMSE [°C]	**r_P**	**ρ_{Sp}**	**τ_k**
T Max	2.247	0.946	0.941	0.800
T Mean	1.852	0.965	0.961	0.840
T Min	2.142	0.956	0.952	0.822

Table S4. Model's performances evaluation within the calibration period 1980-99 and the validation periods (1961-79 and 2000-2022). RMSE, Pearson correlation coefficient, Rank based Spearman and Kendall coefficients were reported about the 10 backup stations and for the ensemble simulation.

Figures

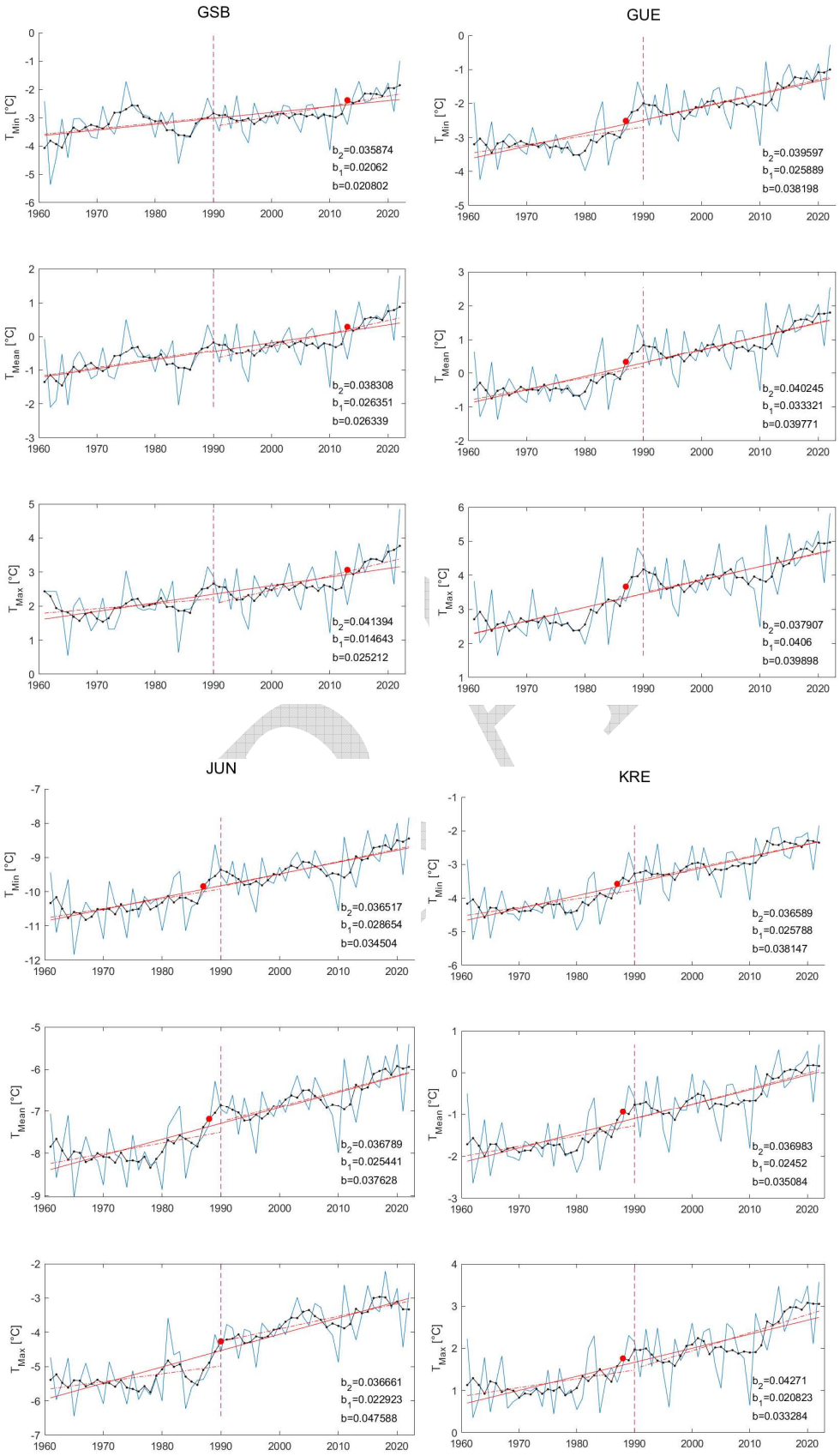
GSB
GUE
JUN
KRE
T_Min [°C]
T_Mean [°C]
T_Max [°C]
b2=0.035874
b1=0.02062
b=0.020802
b2=0.039597
b1=0.025889
b=0.038198
b2=0.038308
b1=0.026351
b=0.026339
b2=0.040245
b1=0.033321
b=0.039771
b2=0.041394
b1=0.014643
b=0.025212
b2=0.037907
b1=0.0406
b=0.039898
b2=0.036517
b1=0.028654
b=0.034504
b2=0.036589
b1=0.025788
b=0.038147
b2=0.036789
b1=0.025441
b=0.037628
b2=0.036983
b1=0.02452
b=0.035084
b2=0.036661
b1=0.022923
b=0.047588
b2=0.04271
b1=0.020823
b=0.033284

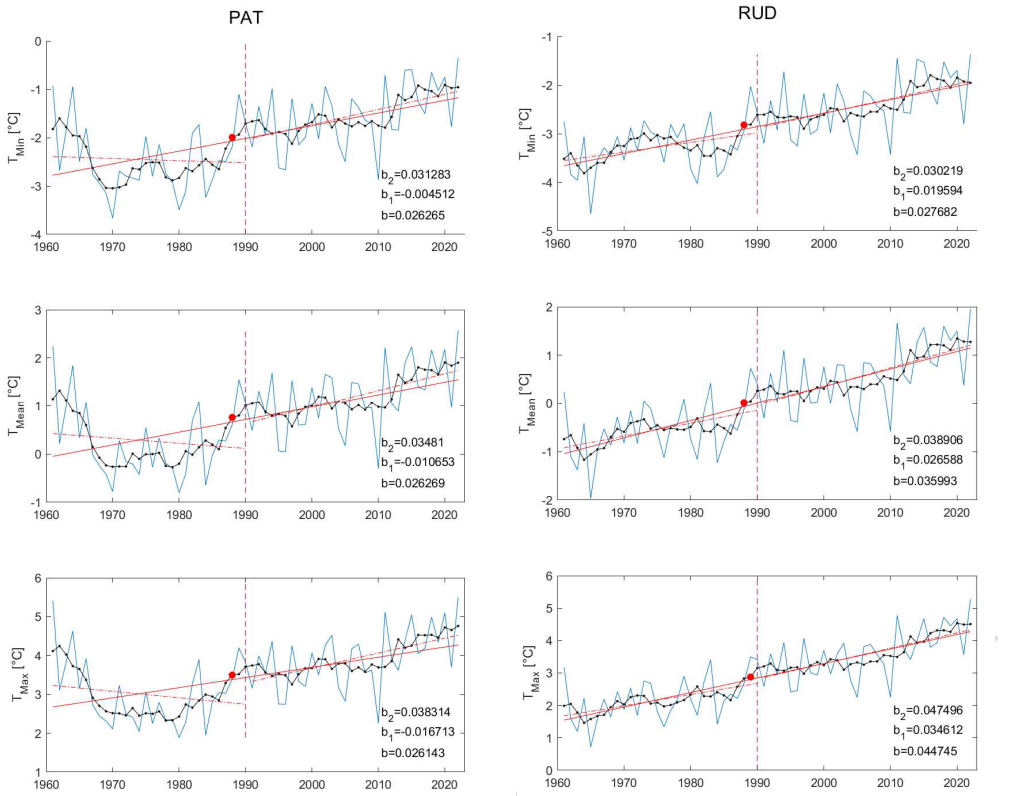
PAT
RUD
T_Min [°C]
b2=0.031283
b1=-0.004512
b=0.026265
b2=0.030219
b1=0.019594
b=0.027682
T_Mean [°C]
b2=0.03481
b1=-0.010653
b=0.026269
b2=0.038906
b1=0.026588
b=0.035993
T_Max [°C]
b2=0.038314
b1=-0.016713
b=0.026143
b2=0.047496
b1=0.034612
b=0.044745

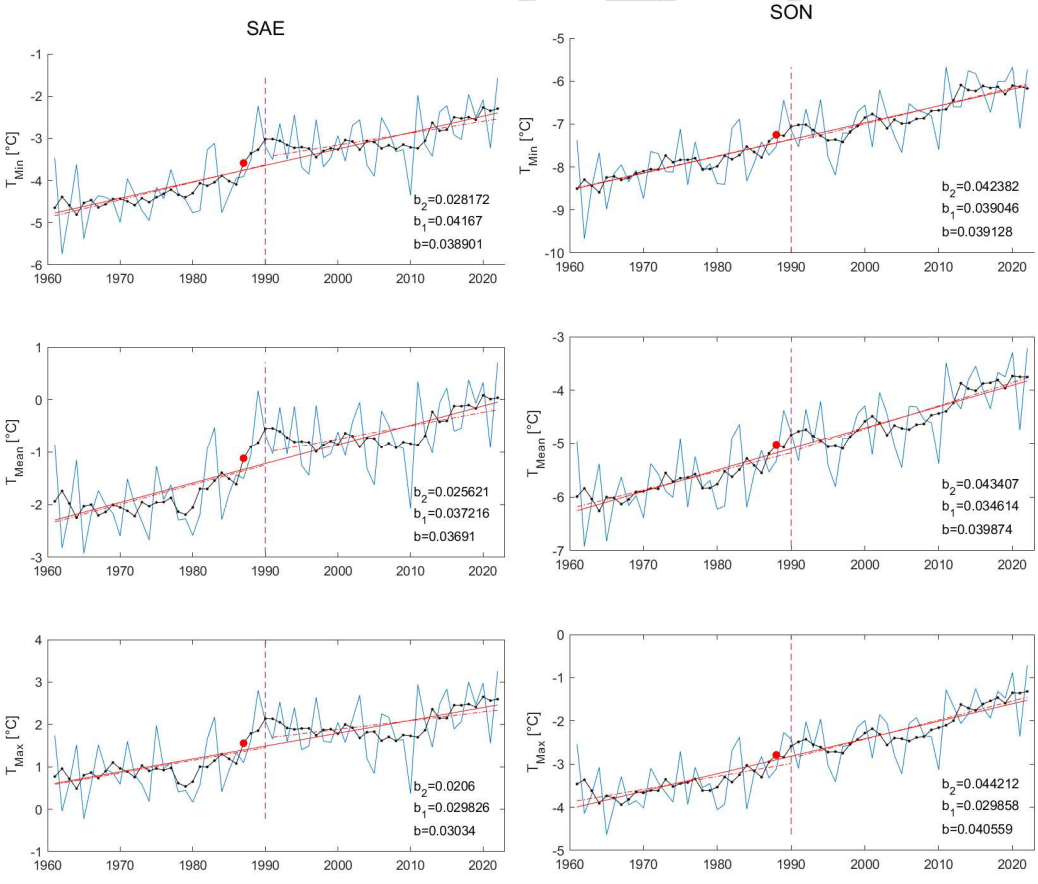
SAE
SON
T_Min [°C]
b2=0.028172
b1=0.04167
b=0.038901
b2=0.042382
b1=0.039046
b=0.039128
T_Mean [°C]
b2=0.025621
b1=0.037216
b=0.03691
b2=0.043407
b1=0.034614
b=0.039874
T_Max [°C]
b2=0.0206
b1=0.029826
b=0.03034
b2=0.044212
b1=0.029858
b=0.040559

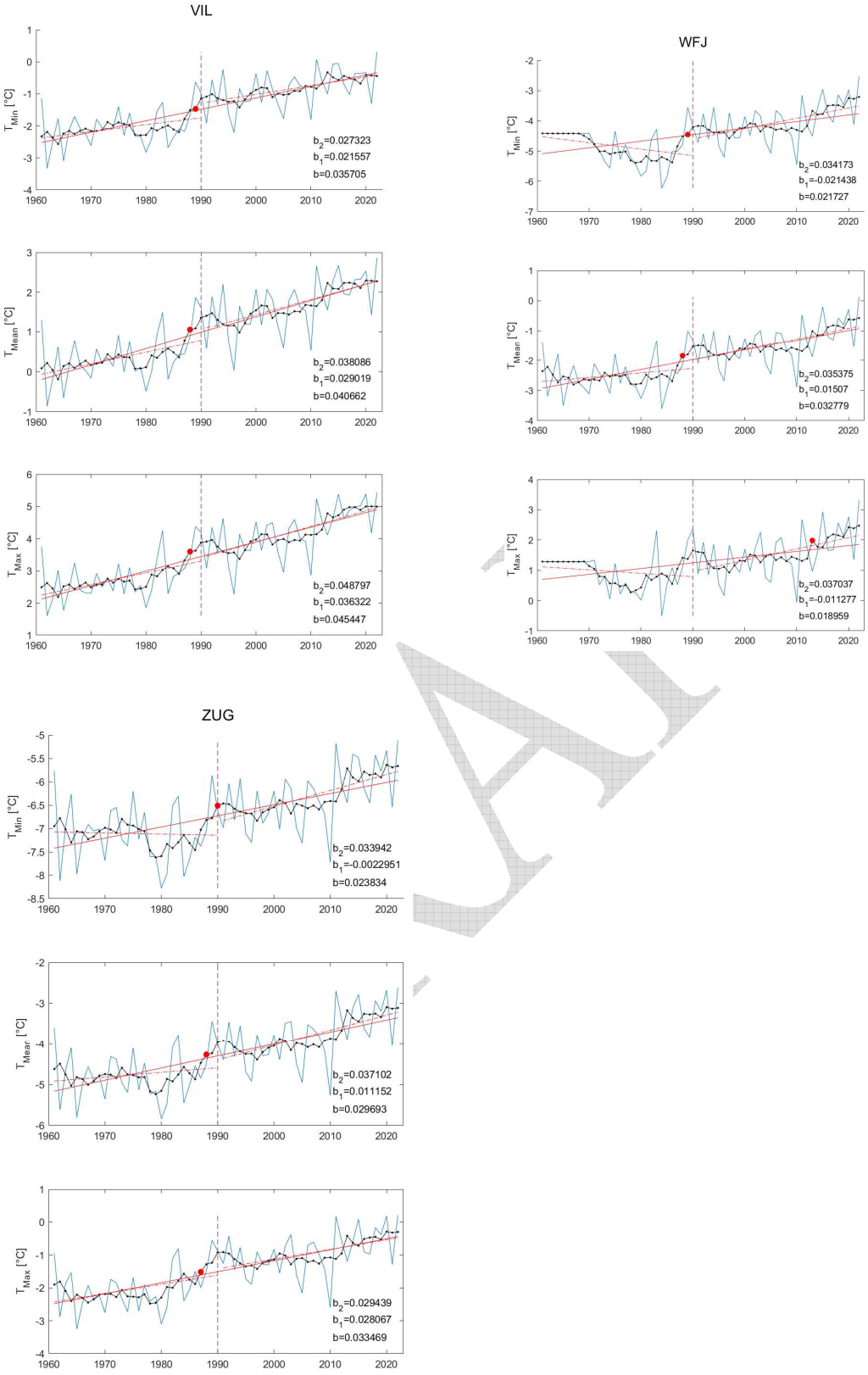

105

Figure S1. Trend Analysis of the mean yearly annual temperature observed time series. Blue lines indicate annual mean, black dot lines the 5 years moving average, the red lines the 1961-2022 trend, the dashed red lines the 1961-1990 and 1991-2022 trends. Red dots show the year of the change point detection.

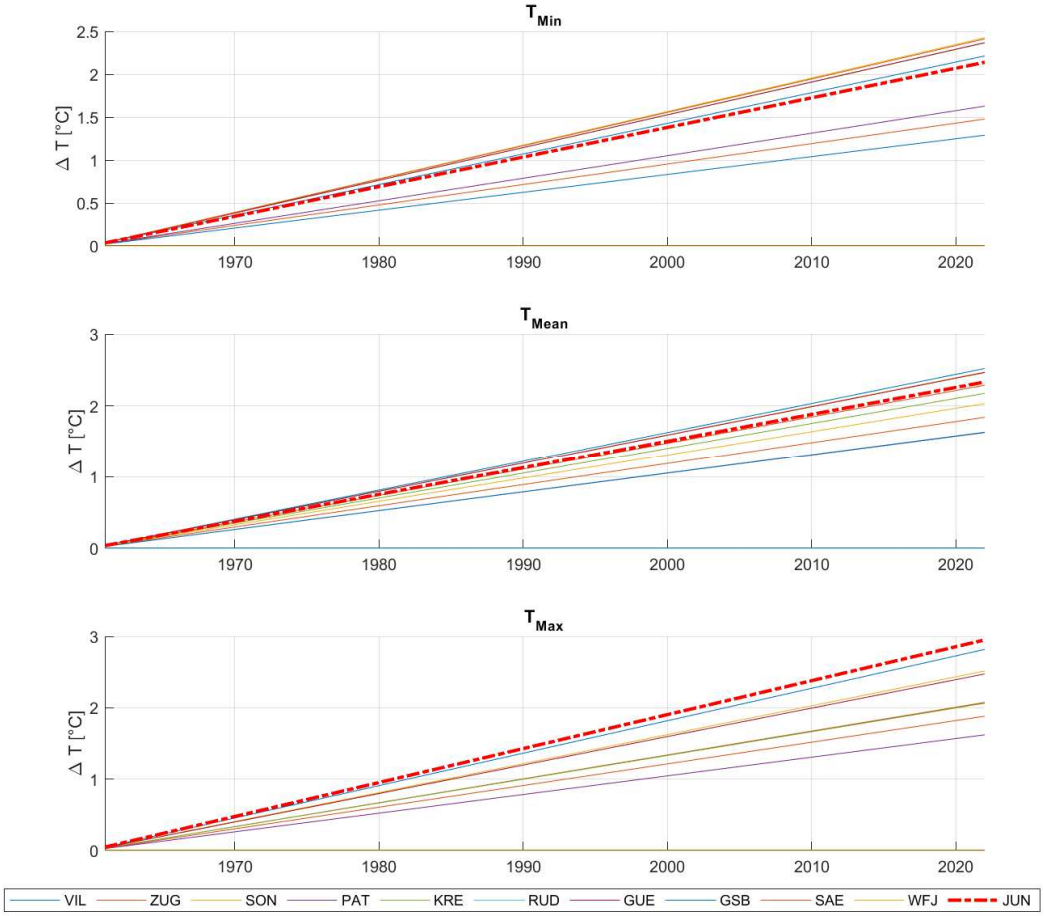

110

Figure S2. Trend Analysis of the mean annual temperature observed time series: comparison among the different stations for minimum, mean and maximum temperature within the period 1961-2022.

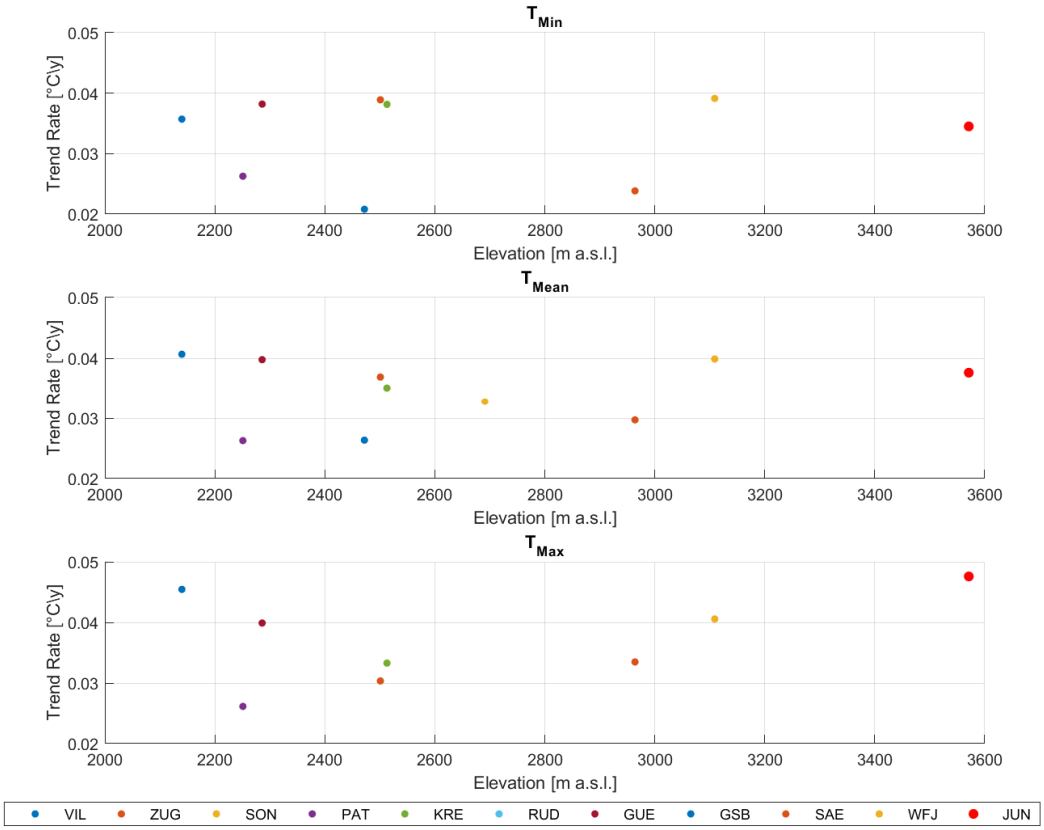

115 **Figure S3. Trend Analysis of the mean annual temperature observed time series against the meteorological stations elevation within the period 1961-2022.**

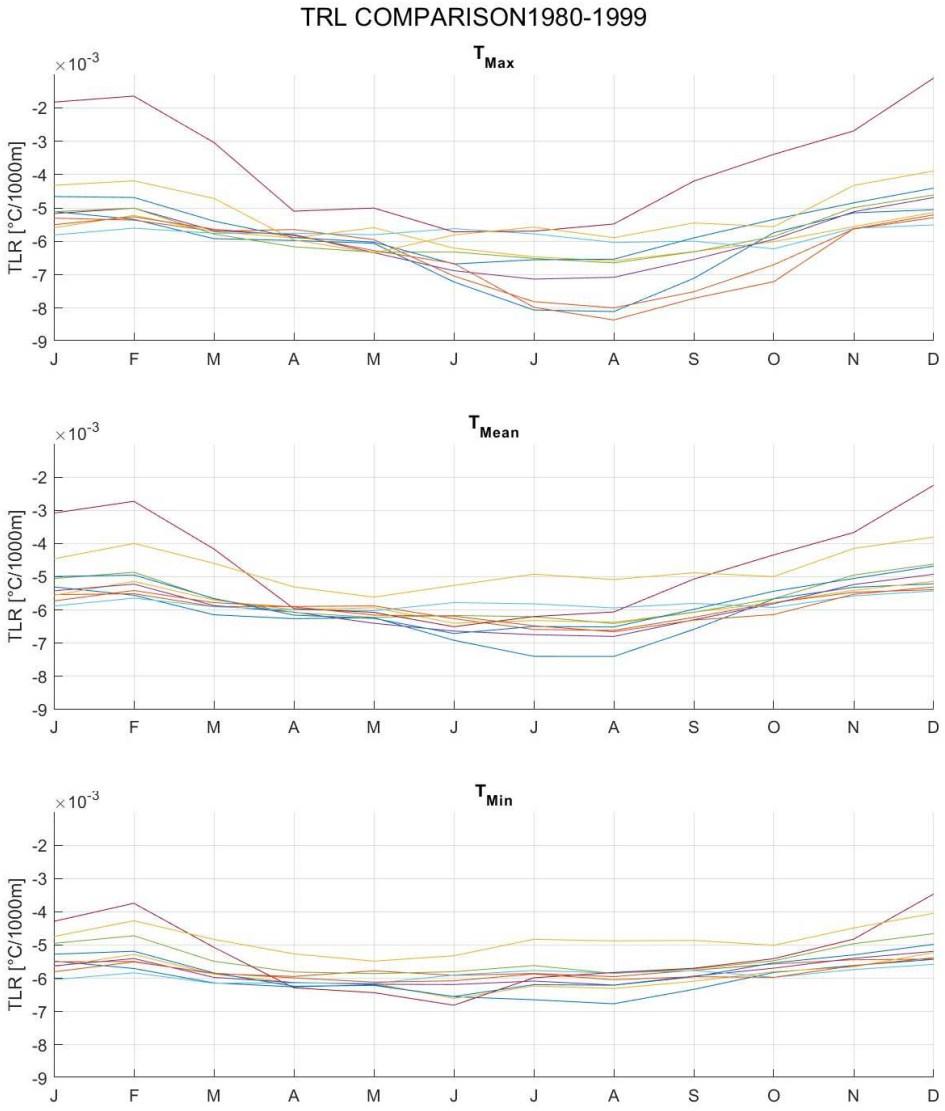

120

Figure S4. TLR comparison among 10 back-up stations related to the calibration period 1980-1999.

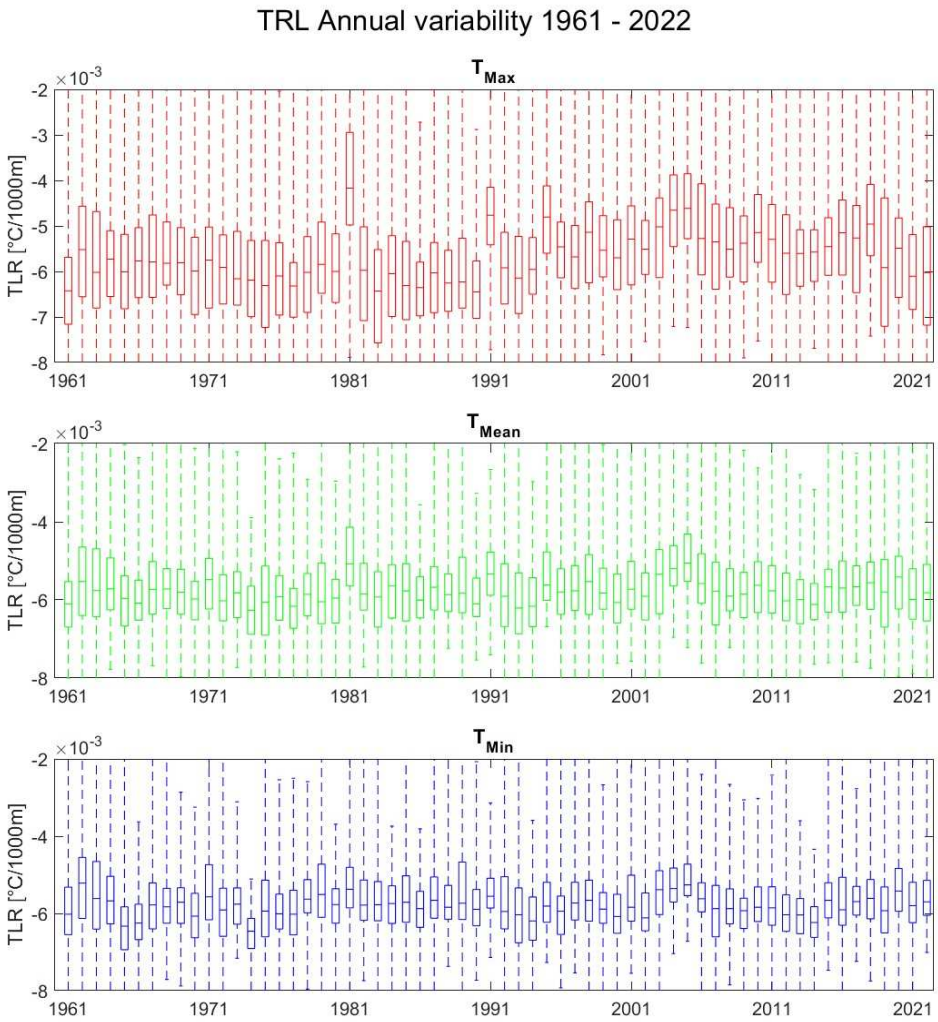

125 **Figure S5. TLR Annual variability within the period 1961-2022 considering all the 10 back-up stations, and all of the 12 months (within each year and each month and related to each station the optimal value of TLR is that minimized the sum of squared errors).**

REFERENCES

Ahmad, M.F., Rasul, G. (2008). Prediction of soil temperature by air temperature; a case study for Faisalabad. Pakistan Journal of Meteorology Vol, 5(9), 19-27.

Auer I, Bohm R, Schoner W. (2001). Long climatic time series from Austria. History and Climate – Memories of the future? Jones PD, Ogilvie AEJ, Davies TD, Briffa KR (eds). Kluwer Academic: New York, 125–151.

Auer I, Bohm R, Jurkovic A, Orklik A, Potzmann R, Schoner W, Ungersbock M, Brunetti M, Nanni T, Maugeri M, Briffa K, Jones P, Efthymiadis D, Mestre O, Moisselin JM, Begert M, Brazdil R, Bochnice O, Cegnar T, Gajic-Capka M, Zaninovic K, Majstorovic Z, Szalai S, Szentimrey T, Mercalli L. (2005). A new instrumental precipitation dataset for the greater Alpine region for the period 1800–2002. International Journal of Climatology 25: 139–166.

Auer, I., R. Böhm, A. Jurkovic, W. Lipa, A. Orlik, R. Potzmann, W. Schöner, M. Ungersböck, C. Matulla, K. Briffa, et al. 2007. HISTALP—Historical instrumental climatological surface time series of the Greater Alpine Region. International Journal of Climatology 27:17–46. doi:10.1002/(ISSN)1097-0088.

Barnett, T., Adam, J., Lettenmaier, D. (2005). Potential impacts of a warming climate on water availability in snow-dominated regions. Nature 438, 303–309. https://doi.org/10.1038/nature04141

Begert M, Schlegel T, Kirchhofer W. (2005). Homogeneous temperature and precipitation series of Switzerland from 1864 to 2000. International Journal of Climatology 25: 65–80.

Beniston M, Jungo P. (2002). Shifts in the distribution of pressure, temperature and moisture and changes in the typical weather patterns in the Alpine region in response to the behavior of the North Atlantic Oscillation. Theoretical and Applied Climatology 71: 29–42.

Beniston, M. (2005). Mountain Climates and Climatic Change: An Overview of Processes Focusing on the European Alps. Pure Appl. Geophys. 162, 1587–1606. https://doi.org/10.1007/s00024-005-2684-9

Beniston M., Stoffel M. (2014). Assessing the impacts of climatic change on mountain water resources, Sci. Total Environ., 493,1129-1137, https://doi.org/10.1016/j.scitotenv.2013.11.122

Beniston, M., Farinotti, D., Stoffel, M., Andreassen, L. M., Coppola, E., Eckert, N., Fantini, A., Giacona, F., Hauck, C., Huss, M., Huwald, H., Lehning, M., López-Moreno, J.-I., Magnusson, J., Marty, C., Morán-Tejéda, E., Morin, S., Naaim, M., Provenzale, A., Rabatel, A., Six, D., Stötter, J., Strasser, U., Terzago, S., and Vincent, C. (2018). The European mountain cryosphere: a review of its current state, trends, and future challenges, The Cryosphere, 12, 759–794, https://doi.org/10.5194/tc-12-759-2018

Bohm R, Auer I, Brunetti M, Maugeri M, Nanni T, Schoner W. (2001). Regional temperature variability in the European Alps: 1760–1998 from homogenized instrumental time series. International Journal of Climatology 21: 1779–1801.

Caty F. Clifton, Kate T. Dayb Charles H. Luce, Gordon E. Grant, Mohammad Safeeq, Jessica E. Halofsky, Brian P. Staab (2018). Effects of climate change on hydrology and water resources in the Blue Mountains, Oregon, USA, Climate Services 10 (2018) 9–19, https://doi.org/10.1016/j.cliser.2018.03.001.

Ceppi P, Scherrer SC, Fischer AM, Appenzeller C. (2012). Revisiting Swiss temperature trends 1959–2008. Int. J. Climatol.; 32: 203–13.

Cos, J., Doblas-Reyes, F., Jury, M., Marcos, R., Bretonnière, P.-A., Samsó, M. (2022). The Mediterranean climate change hotspot in the CMIP5 and CMIP6 projections, Earth Syst. Dynam., 13, 321–340, https://doi.org/10.5194/esd-13-321-2022.

Cristofanelli, P., Fratticioli, C., Hazan, L., Chariot, M., Couret, C., Gazetas, O., Kubistin, D., Laitinen, A., Leskinen, A., Laurila, T., Lindauer, M., Manca, G., Ramonet, M., Trisolino, P., Steinbacher, M. (2023). Identification of spikes in continuous ground-based in situ time series of CO2, CH4 and CO: an extended experiment within the European ICOS Atmosphere network, Atmos. Meas. Tech., 16, 5977–5994, https://doi.org/10.5194/amt-16-5977-2023.

Frei, C. (2014), Interpolation of temperature in a mountainous region using nonlinear profiles and non-Euclidean distances. Int. J. Climatol., 34: 1585-1605. https://doi.org/10.1002/joc.3786

Gleeson E., Greenwood G. B. (2015). "Big Data Are All the Rage—For Mountains, Too," Mountain Research and Development, 35(1), 87-89, (1 February 2015).

Gobiet A., Kotlarski S., Beniston M., Heinrich G., Rajczak J., Stoffel M. (2014). 21st century climate change in the European Alps—A review, Science of The Total Environment, 493, 1138-1151, https://doi.org/10.1016/j.scitotenv.2013.07.050.

Jobst, A.M., Kingston, D.G., Cullen, N.J. and Sirguey, P. (2017). Combining thin-plate spline interpolation with a lapse rate model to produce daily air temperature estimates in a data-sparse alpine catchment. Int. J. Climatol., 37: 214-229. https://doi.org/10.1002/joc.4699

Kleidon, A., Renner, M. (2013). A simple explanation for the sensitivity of the hydrologic cycle to surface temperature and solar radiation and its implications for global climate change, Earth Syst. Dynam., 4, 455–465, https://doi.org/10.5194/esd-4-455-2013.

Kotlarski, S., Bosshard, T., Lüthi, D. et al. Elevation gradients of European climate change in the regional climate model COSMO-CLM. Climatic Change 112, 189–215 (2012). https://doi.org/10.1007/s10584-011-0195-5

Hurrell J.W., Kushnir Y., Ottersen G., Visbeck M. (eds). (2003). The North Atlantic Oscillation: Climate Significance and Environmental Impact, Geophysical Monograph Series 134: American Geophysical Union, Washington, DC.

Imfeld, N., Pfister, L., Brugnara, Y., and Brönnimann, S. (2023). A 258-year-long data set of temperature and precipitation fields for Switzerland since 1763, Clim. Past, 19, 703–729, https://doi.org/10.5194/cp-19-703-2023.

Immerzeel, W.W., Lutz, A.F., Andrade, M. et al. (2020). Importance and vulnerability of the world's water towers. Nature 577, 364–369. https://doi.org/10.1038/s41586-019-1822-y

IPCC (2019). IPCC Special Report on the Ocean and Cryosphere in a Changing Climate [H.-O. Pörtner, D.C. Roberts, V. Masson-Delmotte, P. Zhai, M. Tignor, E. Poloczanska, K. Mintenbeck, A. Alegría, M. Nicolai, A. Okem, J. Petzold, B. Rama, N.M. Weyer (eds.)]. Cambridge University Press, Cambridge, UK and New York, NY, USA, 755 pp. https://doi.org/10.1017/9781009157964.

Lute AC, Abatzoglou JT. (2021). Best practices for estimating near-surface air temperature lapse rates. Int J Climatol.; 41 (Suppl. 1): E110–E125. https://doi.org/10.1002/joc.6668

Mountain Research Initiative EDW Working Group (2015). Elevation-dependent warming in mountain regions of the world. Nature Climate Change 5(5):424-430, https://doi.org/10.1038/nclimate2563

Navarro-Serrano F, López-Moreno JI, Azorin-Molina C, et al. (2018). Estimation of near-surface air temperature lapse rates over continental Spain and its mountain areas. Int J Climatol.; 38: 3233–3249. https://doi.org/10.1002/joc.5497

Ohmura, A. (2012). Enhanced temperature variability in high-altitude climate change. Theoretical and Applied Climatology, 110, 499-508.

Pepin, N. C., and J. R. Norris (2005), An examination of the differences between surface and free-air temperature trend at high-elevation sites: Relationships with cloud cover, snow cover, and wind, J. Geophys. Res., 110, D24112, doi:10.1029/ 2005JD006150.

Pepin, N. C., Arnone, E., Gobiet, A., Haslinger, K., Kotlarski, S., Notarnicola, C., et al. (2022). Climate changes and their elevational patterns in the mountains of the world. Reviews of Geophysics, 60, e2020RG000730. https://doi.org/10.1029/2020RG000730

Philipona, R. (2013). Greenhouse warming and solar brightening in and around the Alps. Int. J. Climatol., 33: 1530-1537. https://doi.org/10.1002/joc.3531

Rangwala, I. Miller, J. (2012). Climate change in mountains: a review of elevation-dependent warming and its possible causes, Climatic Change, 114(3) 527-547.

Rantanen, M., Karpechko, A.Y., Lipponen, A. et al. (2022). The Arctic has warmed nearly four times faster than the globe since 1979. Commun Earth Environ 3, 168. https://doi.org/10.1038/s43247-022-00498-3

Rolland, C. (2003). Spatial and Seasonal Variations of Air Temperature Lapse Rates in Alpine Regions. Journal of Climate 16(7) pp. 1032-1046. Available at: https://journals.ametsoc.org/view/journals/clim/16/7/1520-0442_2003_016_1032_sasvoa_2.0.co_2.xml [Accessed 10 Apr 2024]

Romeo, R., Vita, A., Mnauelli S., Zanini, E., Freppaz, M., Stanchi, S. (2015). Understanding Mountain Soils: A contribution from mountain areas to the International Year of Soils 2015.

Sheldon, K.S., Tewksbury, J.J. (2014). The impact of seasonality in temperature on thermal tolerance and elevational range size. Ecology, 95: 2134-2143. https://doi.org/10.1890/13-1703.1

Scherrer, S., Ceppi, P., Croci-Maspoli, M., Appenzeller, C. (2012). Snow- albedo feedback and Swisss spring temperature trends, Theoretical and Applied Climatology, 110, 509–516, https://doi.org/10.1007/s00704-012-0712-0

Smith, N.G., Dukes, J.S. (2013). Plant respiration and photosynthesis in global-scale models: incorporating acclimation to temperature and CO2. Glob Change Biol, 19, 45-63. https://doi.org/10.1111/j.1365-2486.2012.02797 .

Shepherd T. G. (2003). Large-Scale Atmospheric Dynamics for Atmospheric Chemists. Chemical Reviews 2003 103 (12), 4509-4532 https://doi.org/10.1021/cr020511z

Singh S. P., Thadani R. (2015). Complexities and Controversies in Himalayan Research: A Call for Collaboration and Rigor for Better Data, Mountain Research and Development 35(4), 401-409, https://doi.org/10.1659/MRD-JOURNAL-D-15-00045

Tudoroiu, M.; Eccel, E.; Gioli, B.; Gianelle, D.; Schume, H.; Genesio, L.; Miglietta, F. (2016). Negative elevation-dependent warming trend in the Eastern Alps. Environmental Research Letters, 11 (4): 044021. https://doi.org/10.1088/1748-9326/11/4/044021

Viviroli, D., Archer, D. R., Buytaert, W., Fowler, H. J., Greenwood, G. B., Hamlet, A. F., Huang, Y., Koboltschnig, G., Litaor, M. I., López-Moreno, J. I., Lorentz, S., Schädler, B., Schreier, H., Schwaiger, K., Vuille, M., Woods, R. (2011). Climate change and mountain water resources: overview and recommendations for research, management and policy, Hydrol. Earth Syst. Sci., 15, 471–504, https://doi.org/10.5194/hess-15-471-2011.

Viviroli, D., H. H. Du¨rr, B. Messerli, M. Meybeck, R. Weingartner (2007). Mountains of the world, water towers for humanity: Typology, mapping, and global significance, Water Resour. Res., 43, W07447, https://doi.org/10.1029/2006WR005653.

Wang, Q., Fan, X., Wang, M. (2016). Evidence of high-elevation amplification versus Arctic amplification. Sci Rep 6, 19219. https://doi.org/10.1038/srep19219

Wang, J., Zhang, M., Wang, S. et al. (2016). Decrease in snowfall/rainfall ratio in the Tibetan Plateau from 1961 to 2013. J. Geogr. Sci. 26, 1277–1288. https://doi.org/10.1007/s11442-016-1326-8

Wanner H, Bronnimann S, Casty C, Gyalistras D, Luterbacher J, Schmutz C, Stephenson DB, Xoplaki E. (2001). North Atlantic oscillation – concepts and studies. Surveys in Geophysics 22: 321–382.

World Meteorological Organization (2022). Centennial Observing Stations State of Recognition Report – 2021. Technical report, WMO-No. 1296, (2022). ISBN 978-92-63-11296-5, https://library.wmo.int/idurl/4/58048